Two metamorphic cycles recorded by monazite in eclogite-facies gneisses (Southern Armorican Massif, France): A Cambro-Ordovician continental crust involved in eo-Variscan subduction

Valérie Bosse, Gaston Godard, Jean-Luc Devidal, Julie Mallens, Thomas Shea

BSGF - Earth Sciences Bulletin 2024, 195, 20
© V. Bosse *et al.*, Published by EDP Sciences 2024
https://doi.org/10.1051/bsgf/2024018

BSGF
Earth Sciences Bulletin
Available online at:
www.bsgf.fr

Two metamorphic cycles recorded by monazite in eclogite-facies gneisses (Southern Armorican Massif, France): A Cambro-Ordovician continental crust involved in eo-Variscan subduction

Valérie Bosse[1], Gaston Godard[2], Jean Luc Devidal[1], Julie Mallens[1] and Thomas Shea[3,*]

[1] UMR 6524, Laboratoire Magmas – Volcans, Université Blaise Pascal, Clermont Ferrand
[2] Institut de Physique du Globe de Paris, Université de Paris-Cité, Paris
[3] Dept. of Earth Sciences, University of Hawaii at Mānoa

Received: 16 March 2024 / Accepted: 26 August 2024 / Publishing online: 11 October 2024

Abstract – We present U-Th/Pb data obtained for xenotime and monazite from the polycyclic eclogite-facies para- and ortho-gneisses of the Les Essarts Unit (Vendée, southern Armorican Massif, France), which have recorded an HT-LP cycle ending with a first retrogression and a subsequent HP eclogite-facies metamorphism similar to that of the neighbouring eclogites. Some paragneisses and orthogneisses are only slightly deformed and retrogressed, showing the structure of nebulitic migmatite or metagranite, respectively; both show well-preserved complex coronitic and pseudomorphic microstructures, due to the eclogite-facies metamorphism. Monazite I and xenotime crystallised during the HT stage providing an opportunity to date the early HT metamorphic event in the paragneiss and the emplacement of granite in the orthogneiss. U/Pb ages obtained from monazite I and xenotime of the cordierite-bearing migmatitic paragneisses range between 510 and 480 Ma (Late Cambrian-Early Ordovician). These ages may correspond to the crystallisation and/or re-equilibration of monazite and xenotime during the prograde stage of the HT cycle, close to the *T* peak. Consistent monazite and xenotime U/Pb ages around 496 Ma in the orthogneiss represent the age of the granite protolith. During subsequent HP overprint in the gneisses, numerous coronas developed at the expense of the early HT parageneses, in particular plagioclase. In both paragneiss and orthogneiss, monazite I in contact with HT plagioclase reacted to form apatite + zoisite + monazite II coronas. The small monazite II crystals could be dated in a paragneiss sample and gave a lower intercept age of 395 ± 9 Ma, interpreted as the age of the eclogite-facies HP metamorphism. This age is in agreement with those obtained in HP metamorphic rocks of the Upper Allochthon Unit of the Iberian-Armorican Arc (Bragança, Cabo-Ortegal, Audierne) representing the first evidence of convergence in the Variscan cycle.

Keywords: Monazite dating / polycyclic metamorphism / Armorican Massif / eclogite-facies metamorphism / Ibero-Armorican Arc / Variscan belt

Résumé – Deux cycles métamorphiques enregistrés par la monazite de gneiss de faciès éclogite (domaine sud armoricain, France) : une croûte continentale cambro-ordovicienne impliquée dans la subduction éo-varisque. Nous présentons des âges U-Th/Pb obtenus pour le xénotime et la monazite des paragneiss et orthogneiss polycycliques de l'unité des Essarts (Vendée, domaine sud armoricain, France), qui ont enregistré un cycle de HT-BP se terminant par une première phase de rétromorphose, suivi d'un métamorphisme postérieur dans le faciès éclogite, semblable à celui des éclogites voisines. Certains paragneiss et orthogneiss sont très peu déformés et rétromorphosés, montrant respectivement la structure initiale d'une migmatite nébuleuse ou d'un métagranite. Ils présentent tous des textures coronitiques et des pseudomorphoses complexes formées au cours du métamorphisme en faciès éclogite. La monazite I et le xénotime ont cristallisé pendant le stade de HT, ce qui permet de dater ce métamorphisme précoce dans le paragneiss, et la mise en place du granite dans l'orthogneiss. Les âges U/Pb obtenus dans la monazite I et le xénotime des paragneiss migmatitiques à cordiérite se situent entre 510 et 480 Ma (fin du Cambrien-début de l'Ordovicien). Cet intervalle d'âges peut correspondre à la cristallisation et/ou au rééquilibrage de la

*Corresponding author: valerie.bosse@uca.fr

monazite et du xénotime au cours de la phase prograde du cycle de HT, près du pic en température. Les âges U/Pb autour de 496 Ma dans la monazite et le xénotime de l'orthogneiss représentent l'âge du protolithe granitique. Au cours du métamorphisme de HP ultérieur, de nombreuses couronnes se sont développées aux dépens des paragenèses de HT précoces, en particulier le plagioclase. Dans les paragneiss et les orthogneiss, la monazite I en contact avec le plagioclase de HT a réagi pour former des couronnes d'apatite, zoisite et monazite II. Les cristaux de monazite II de très petite taille ont pu être datés dans un échantillon de paragneiss et ont donné un âge de 395 ± 9 Ma, interprété comme l'âge du métamorphisme de HP dans le faciès éclogite. Cet âge est en accord avec ceux obtenus dans les roches métamorphiques de HP de l'unité Allochtone Supérieure de l'Arc ibéro-armoricain (Bragance, Cabo-Ortegal, Audierne) qui représentent les premières manifestations de la convergence du cycle varisque.

Mots-clés : datation monazite / métamorphisme polycyclique / massif armoricain / métamorphisme en faciès éclogite / Arc Ibéro-armoricain

1 Introduction

The record of polycyclic metamorphic evolution is well established in recent collisional chains such as the Alps, where evidence for earlier Variscan events has long been recognised (*e.g.*, Le Bayon *et al.*, 2006; Cenki-Tok *et al.*, 2011; Nosenzo *et al.*, 2021). In other contexts, the preservation of two (or more) orogenic cycles within the rock record is open to debate. Indeed, polycyclic evolution is not always easy to distinguish from polymetamorphic evolution, which is characterised by a continuous evolution of *P-T* conditions during a single orogenic cycle. While structural and petrological studies can help in establishing successive orogenic events, key evidence often comes from geochronological data, when these events are separated by a span of time well beyond the estimated duration of an orogenic cycle. Only the ability to date mineralogical reactions *in situ* and in their textural context can shed light on this type of problem, which has large-scale consequences for the evolution of tectono-metamorphic units during orogenesis. The use of geochronometers as faithful petrological and kinematic markers (hygrochronometers as defined by Villa, 2016) is therefore essential.

The Variscan belt of western and central Europe contains eclogite-facies rocks that are thought to have formed during eo-Variscan subduction. However, estimates of the age of associated ophiolites and their high-*P* (HP) metamorphism have given widely scattered results and remain debated. To date, the geodynamic history preceding the subduction events also remains poorly understood or investigated. Initially, studies aimed at determining the age of HP events were based on U/Pb dating of zircon yielding widely scattered ages ranging from the Cambrian to the Lower Silurian (*e.g.*, Gebauer *et al.*, 1981; Peucat *et al.*, 1982; Berger *et al.*, 2010; Whitney *et al.*, 2015). However, it is now clear that zircon evolution is difficult to connect with the metamorphic history, and clear evidence for metamorphic zircon overgrowths contemporaneous with the eclogite-facies event is generally lacking (Paquette *et al.*, 2017; Pitra *et al.*, 2022). Recent studies have re-examined the age of eclogites in the western Variscan belt, particularly in the French Massif Central (Lotout *et al.*, 2018, 2020; de Marien *et al.*, 2023), using geochronometers such as U-Th/Pb in monazite, U/Pb in rutile or titanite, and Lu/Hf and/or Sm/Nd in garnet. By combining trace element analysis with in-situ dating of accessory and major phases, the dates have been interpreted in relation to the petrological evolution of the sample. The results constrain the age range of the subduction events, and better define the age of the metamorphic events in this area at around 380–360 Ma. In the Armorican Massif, ages of HP metamorphism obtained by zircon U/Pb dating also range from 440 Ma to 355 Ma (Peucat *et al.*, 1982; Paquette *et al.*, 1985; Paquette, 1987; see Ballèvre *et al.*, 2009 for a detailed review). Paquette *et al.* (2017) have re-examined the zircon previously analysed by isotope dilution thermal ionisation mass spectrometry (ID-TIMS), mostly multigrain fractions, using the in-situ laser ablation inductively coupled plasma mass spectrometry (LA-ICPMS) method. Their results led to the conclusion that "no high-pressure event at the previously assumed date of 400–410 Ma is confirmed in any studied zircon grain" and that the "old concept of a Siluro-Devonian eclogite-facies event is most probably related to analytical limitations of the published ages in the 1980s, which led to geodynamic overinterpretations" (Paquette *et al.*, 2017). Although the latter study is a fundamental contribution to the interpretation of the zircon ages obtained by ID-TIMS in HP metamorphic rocks, the ages of the HP metamorphism in the Armorican Massif obtained using various other methods, such as Sm/Nd Grt ages of 362 ±25 Ma in the Champtoceaux complex (Bosse *et al.*, 2000) and Rb/Sr and $^{40}Ar/^{39}Ar$ ages of 358–366 Ma in well-preserved blueschists from the Ile de Groix (Bosse *et al.*, 2005), are still debated.

The discovery of polycyclic eclogite-facies gneisses in Les Essarts Unit (Vendée, southern Armorican Massif, France: Fig. 1; Godard, 2009) provides an opportunity for a new approach to HP-metamorphism dating. Petrological evidence has shown that the paragneisses and orthogneisses of this area have undergone a high-*T* (HT) low-*P* (LP) metamorphism, typical of the continental crust, followed by a first retrogression and then the same HP eclogite-facies metamorphism as the neighbouring eclogites (Godard, 2009). These gneisses could therefore represent remnants of a pre-Variscan continental crust (HT migmatites and granites) that was involved in the eo-Variscan convergence and subduction together with the oceanic crust that generated the eclogites (HP overprint). In the gneisses, monazite crystallised during the HT stage and partly recrystallized during the subsequent HP overprint (Godard, 2009), providing an opportunity to date both events. This article is devoted to the geochronology of these polycyclic eclogite-facies gneisses, with the aim of

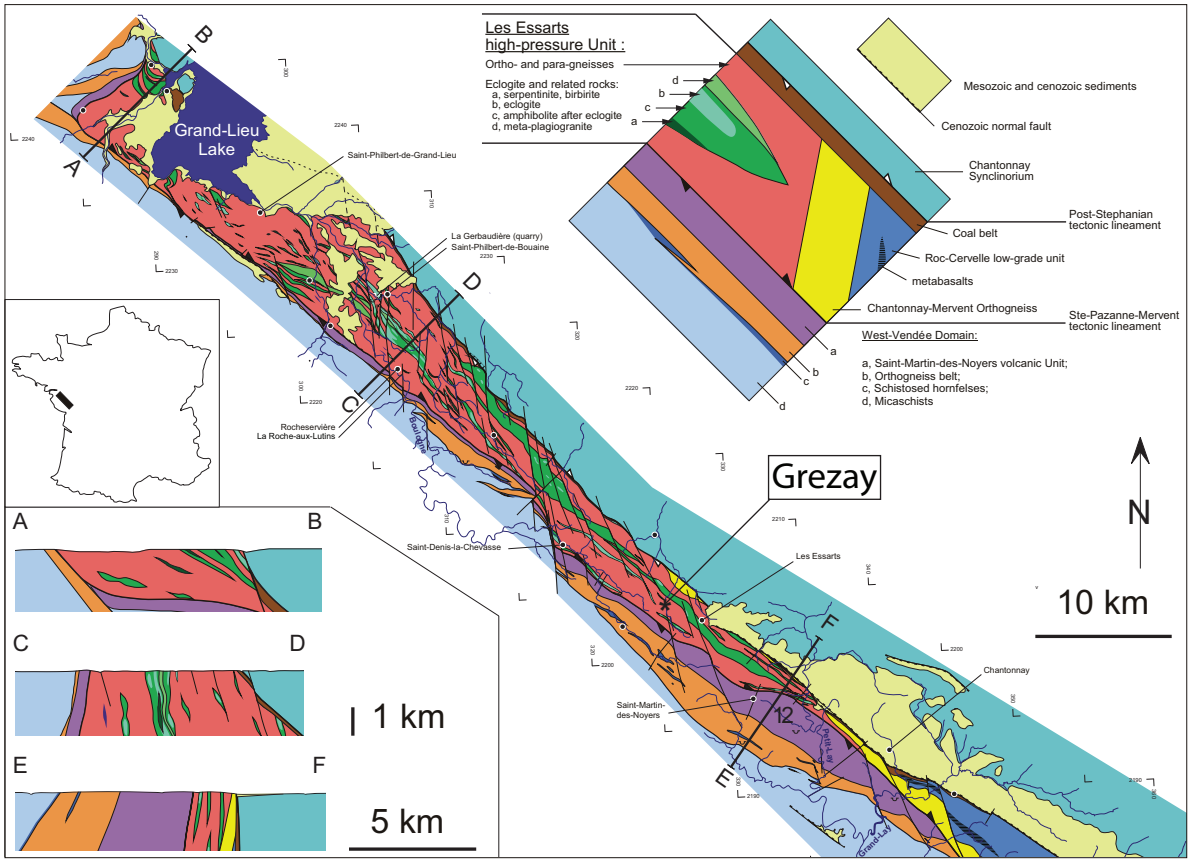

Fig. 1. Geological map of the Les Essarts metamorphic unit (Armorican Massif, France), modified from Godard (2001). The inset block diagram schematically shows the different geological formations and their relationship. All the studied samples come from the Grezay locality.

dating (a) the metamorphic history of the continental slice to which they belonged and (b) the eo-Variscan subduction in which they were involved, prior to their accretion into the Variscan belt.

2 Geological setting and petrology

The Les Essarts HP unit occurs in the Southern Armorican Massif (Vendée, Western France), where it defines a NW–SE-trending zone about 70 km long and a few km wide between two late-Variscan dextral faults, the Vendée coal belt and the Sainte-Pazanne-Mervent tectonic lineament (Fig. 1; *e.g.*, Godard, 2001, 2009; Godard et Bonnet, 2007). It comprises altered ultramafites, eclogites, and eclogite-derived amphibolites, which form several kilometre-long lenses (Fig. 1) that are stretched and boudinaged parallel to the main vertical foliation in the surrounding ortho- and para-gneisses.

2.1 Eclogites

The Vendée eclogites have been considered to be remnants of an old oceanic crust, eclogitised during an eo-Variscan subduction and subsequently incorporated into the Variscan orogenic belt during continental collision (Godard, 1988, 2001, and references therein). Geochemical studies have shown a rather large mineralogical diversity of eclogites, with (i) rare zoisite and kyanite-bearing eclogites derived from Al-Mg rich cumulate gabbros, (ii) abundant quartz-bearing eclogites derived from N-MORB type gabbros, (iii) rutile-rich eclogites derived from Fe-Ti rich gabbros, and (iv) a few more felsic rocks (Godard, 1988, 2001). Weathered ultramafic rocks with rare remnants of garnet peridotite have also been observed (Fig. 1; Godard, 2001). Eclogite-facies conditions were first estimated to be $T = 650–750°C$ and $P > 1.6$ GPa (Godard, 1988). Massone and Li (2022) studied an atoll garnet-bearing eclogite and proposed the existence of two garnet generations reflecting two metamorphic stages close to the pressure peak (stage 1: 2.0 GPa and 550°C and stage 2: 1.8–2.0 GPa and 640°C). A major deformation event occurred during the eclogite-facies metamorphism (Godard and van Roermund, 1995; Mauler *et al.*, 2001), which ended with an almost isothermal evolution at the beginning of the exhumation (Godard, 2001; Massonne and Li, 2022), followed by various retrograde metamorphic reactions that transformed most of the eclogites into amphibolites.

Geochronological studies of zircon from an eclogite sampled at La Gerbaudière quarry (Peucat *et al.*, 1982; Peucat, 1983; Postaire, 1983) gave a discordia age of 436 ± 15 Ma (U/Pb multigrain size-fraction ID-TIMS; lower intercept age), which was then interpreted as the age of the HP metamorphism. Zircon crystals from the very separate used by Peucat *et al.* (1982) were analysed *in situ* by LA-ICPMS dating (Paquette *et al.*, 2017). The results showed the absence of

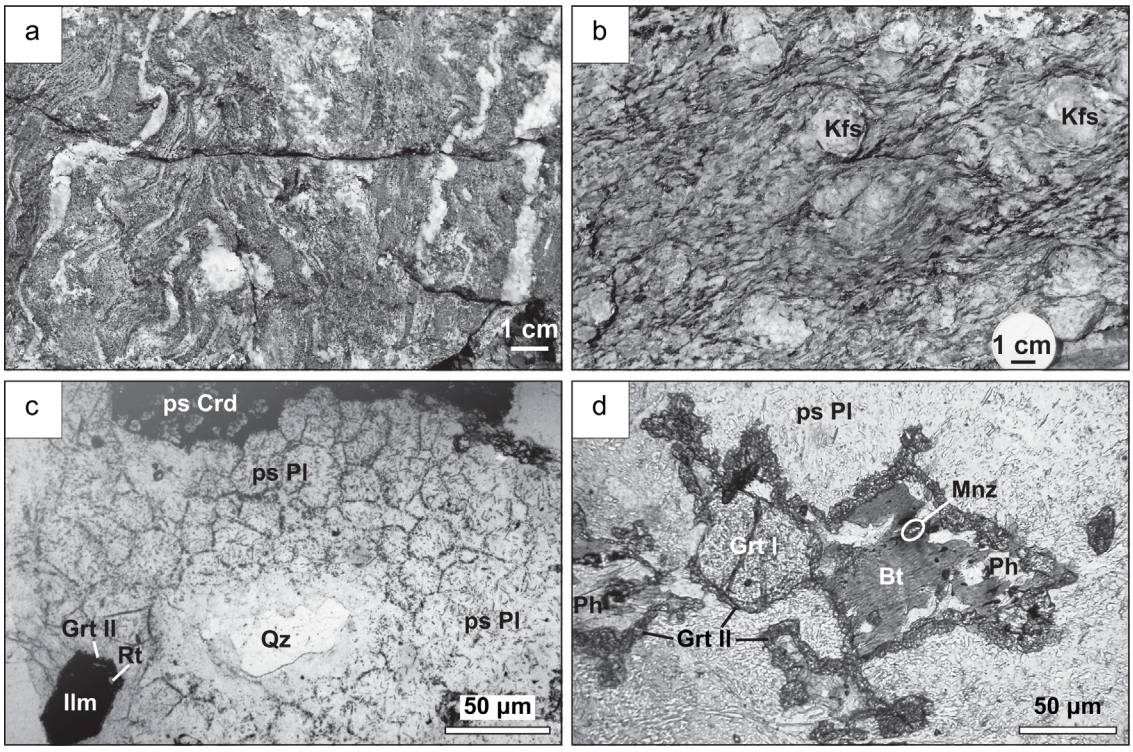

Fig. 2. Coronitic gneisses from Grezay: (a) undeformed migmatite, with eclogite-facies garnet-bearing microcoronas (not visible) (modified after Godard, 2009); (b) orthogneiss, with K-feldspar *augen* (Kfs) and similar microcoronas; (c) micrograph of a paragneiss, showing Grt II+Rt microcoronas around ilmenite (Ilm), pseudomorphs after cordierite (ps Crd) and pseudomorphs after plagioclase (ps Pl); the latter consists of polycrystalline albite and minute kyanite rods delimiting a honeycomb-like structure, the cells of which could represent former plagioclase single crystals before the albite-jadeite transition (plane-polarised light; after Godard, 2009); (d) micrograph of a paragneiss, showing pseudomorphs after plagioclase (ps Pl), Grt II+Ph microcoronas at the interface between biotite (Bt) and the former plagioclase (ps Pl), and Grt II overgrowths at the interface between pre-existing garnet (Grt I) and the former plagioclase; a monazite (Mnz) grain developed a radiohalo in biotite (plane-polarised light).

inherited cores, Th/U ratios of 0.4 ± 0.1 typical of magmatic zircons and yielded a lower intercept age of 487 ± 12 Ma in a Tera-Wasserburg diagram. This age has therefore been assigned to the formation of the gabbroic protolith in an oceanic environment, without a record of the eclogite-facies metamorphism (Paquette *et al.*, 2017). Some of the eclogites were exhumed at the end of the Carboniferous (at about 300 Ma), since eclogite pebbles have been observed in the Stephanian detrital deposits of the Vendée coal belt (Godard, 2001; Godard et Bonnet, 2007).

2.2 Coronitic gneisses

Most of the rocks surrounding the eclogites are schistose and rich in white mica. Their present paragenesis consists of phengitic muscovite, quartz, albitic plagioclase, biotite and, sporadically, garnet and microcline. However, relict parageneses suggest that they are derived from earlier biotite, garnet, quartz, plagioclase and microcline-bearing gneisses, with cordierite in some cases. In a dozen localities listed by Godard (2001), some of these gneisses are exceptionally poorly deformed and retrogressed (Fig. 2). Early parageneses and coronitic structures are then preserved, revealing a complex history.

Two types of gneisses can be distinguished on the basis of their origin:

(a) *Orthogneisses* show the usual paragenesis of a metagranite (Fig. 2b): quartz + oligoclase + biotite + muscovite + microcline. Orthoclase is transformed into perthitic microcline, which can form centimetre-scale *augen*. The main feature of these orthogneisses is the presence of complex garnet-bearing microcrystalline coronas along the plagioclase-biotite and microcline-biotite interfaces.

(b) *Paragneisses* also show numerous coronas that have developed at the expense of a pre-existing cordierite-bearing migmatitic paragenesis (Fig. 2a). The *P-T* conditions of this HT-LP event have been estimated to be ~0.32 GPa and ~670°C in samples from Grezay (Godard, 2009). Commonly, the structure of the paragneisses is that of a nebulitic migmatite (Fig. 2a). In the Grezay area, migmatisation is also evidenced by the common occurrence of leucosomes composed of Qz + Pl + Kfs + Bt ± Crd (± tourmaline ± Ilm ± monazite). The melanosome generally includes Bt + Qz + Crd + Grt + Pl + Ilm (+ F-apatite + monazite), with relics of muscovite and Al-silicate isolated within biotite-rich clusters and pseudomorphs after cordierite, respectively. Biotite, quartz and Al-silicate are always separated from each

other by pseudomorphed cordierite which indicates that cordierite grew at the expense of biotite, quartz and sillimanite, according to a well-known migmatisation reaction: Bt + Qz + Sil (± Pl) → Crd + Melt (+ Grt) (*e.g.*, Waters and Whales, 1984; Le Breton and Thompson, 1988; Stevens *et al.*, 1997).

Numerous coronas can be observed in both types of rock (Fig. 2d). They developed at the expense of the pre-existing migmatitic or granitic parageneses, particularly at the interfaces between feldspars (plagioclase or microcline) and mafic minerals (biotite, ilmenite or cordierite: Fig. 2c-d), but also monazite. Plagioclase commonly forms a microcrystalline mosaic of polycrystalline albite in which minute rodlets of kyanite, and minor zoisite and micas are visible only by scanning electron microscopy (SEM). The kyanite rods are ordinarily arranged in trails that delineate polygonal millimetre-sized cells with a honeycomb-like structure (Fig. 2c), which is interpreted by Godard (2009) as the silhouettes of the former plagioclase single crystals of the HT paragenesis. This type of recrystallisation without deformation would be explained by phase transitions: Oligoclase → X + minor zoisite and kyanite, followed by the retrograde reaction X → albite; indeed, X could be jadeite, which, however, has never been observed. This second episode occurred in eclogite-facies conditions at $P > 1.6$ GPa and $T \approx 700$°C (Godard, 2009).

Two lines of evidence indicate that the HT event and the subsequent HP eclogite-facies overprint were separated by a first retrogression at $T < 400$°C: K-feldspar exsolved perthitic lamellae and cordierite was altered to pinite before the formation of the HP coronas, indicating a polycyclic rather than polymetamorphic *P-T* evolution for these rocks.

Although the eclogites and ultramafites have been considered to be remnants of an oceanic lithosphere, the surrounding ortho- and para-gneisses clearly belong to a continental crust. This led Godard (1983, 2001) to interpret the Les Essarts Unit as a possible tectonic melange of pre-Hercynian continental and oceanic crusts that were eclogitised during eo-Variscan subduction and subsequently incorporated into the Hercynian orogenic belt.

Two samples of the paragneisses from Grezay were studied in the present work: VP7-2 is a piece of the main sample described by Godard (2009), whereas VP7c was sampled in the same disused small quarry. VP7r is an orthogneiss (actually, an almost undeformed metagranite: Fig. 2b) from the same locality (lat. 46.7820; long. −1.2597; Fig. 1).

3 Monazite and xenotime

3.1 Textural characteristics and chemical composition of monazite

In the three samples studied, monazite is common and occurs either as inclusions in garnet, quartz or biotite or at contacts with the plagioclase pseudomorphs described above. Monazite isolated in garnet, quartz or biotite (partially transformed into phengite) consists in pristine prismatic or rounded grains of 10–30 μm in size (Figs. 3e-g, 4a-c, 4e-f). They appear not to have chemically interacted with the host mineral, but show ~20 μm-thick cathodoluminescent halos in quartz, visible under the SEM, revealing lattice damage due to monazite radioactivity. Monazite I crystals at contacts with the plagioclase pseudomorphs commonly reach 50 μm in size, and show complex coronas composed of apatite, zoisite and clusters of small grains of monazite II, both in orthogneiss (sample VP7r: Fig. 5) and in paragneiss (sample VP7-2: Fig. 3a-d). In sample VP7r (Fig. 5), the monazite II crystals are small (<5 μm) compared to sample VP7-2 where their size can reach 20 μm (Fig. 3a-d). In the paragneiss sample VP7c, where large (>100 μm) monazite I grains are commonly subhedral, elongated or round, these monazite crystals show irregular corroded rims at the contacts with the plagioclase pseudomorphs (Fig. 4d), but no clear reaction corona. By contrast, monazite I grains may have been completely replaced by clusters of monazite II associated with apatite and zoisite in the other two samples, in particular VP7-2 (Fig. 3c, d).

The chemical compositions of monazite are reported in Supplementary Material (SM1) and in Figure 6a-b. In all samples, there is no systematic relationship between monazite compositions and textural position. Most of the observed chemical variations are explained by the brabantite substitution ($2\ REE^{3+} = Th^{4+} + Ca^{2+}$) (Fig. 6a), with some huttonite exchange ($REE^{3+} + P^{5+} = Th^{4+} + Si^{4+}$). High-contrast BSE imaging and X-ray mapping (SM5) show that most of the monazite grains, either enclosed in quartz, garnet, micas or in the pseudomorphs after plagioclase, are only slightly zoned, with Y, U and Th showing the most variation (Fig. 6b). However, it is difficult to define a general trend for the core-to-rim zonation of the grains.

Pristine monazites in the studied paragneisses (*i.e.*, monazite in sample VP7c and non-reactive monazite in sample VP7-2) show large variations in Y_2O_3 content (Fig. 6b), with monazites from sample VP7-2 having a higher Y_2O_3 content ($0.42 < Y_2O_3 < 2.02$ wt%) than sample VP7c ($0.11 < Y_2O_3 < 1.75$ wt%). Monazite therefore appears to be more saturated in Y in the case of VP7-2, where it coexists with xenotime, as opposed to VP7c where xenotime is absent. Variations in ThO_2 content are also large, with a slightly wider range and higher content in sample VP7-2 ($2.28 < ThO_2 < 5.49$ wt%) than in sample VP7c ($2.96 < ThO_2 < 4.94$ wt%). In sample VP7-2, the ThO_2 content decreases as Y_2O_3 increases, whereas in sample VP7c both are correlated. Monazite included in garnet and quartz in sample VP7-2 shows large variations in ThO_2 content (between 1.49 and 7.79 wt%) and UO_2 content (between 0.31 and 1.87 wt%) (Fig. 6b). Y_2O_3 is slightly higher in the reacted monazite than in the pristine monazite (between 1.04 and 2.58 wt%). In sample VP7c, the monazite inclusions have a chemical composition almost similar to that of pristine monazites, except for the Y_2O_3 which is slightly higher (2.12 wt%) in the inclusions. In both samples, the inclusions open to the matrix display the same range of compositions as the shielded inclusions. In sample VP7-2, the core of the reactive monazites has Y_2O_3, ThO_2 and UO_2 contents between those of the inclusions and those of the pristine matrix monazite (Fig. 6b). In sample VP7-2, monazite II in the coronas has compositions almost similar to those of pristine monazite in the same samples. A few monazite I grains of the paragneiss samples show inherited nuclei, with a distinct composition (see VP7C-45 and VP7-2-12 in SM5).

Monazite from the orthogneiss sample VP7r has a distinctly different composition from that of the paragneiss

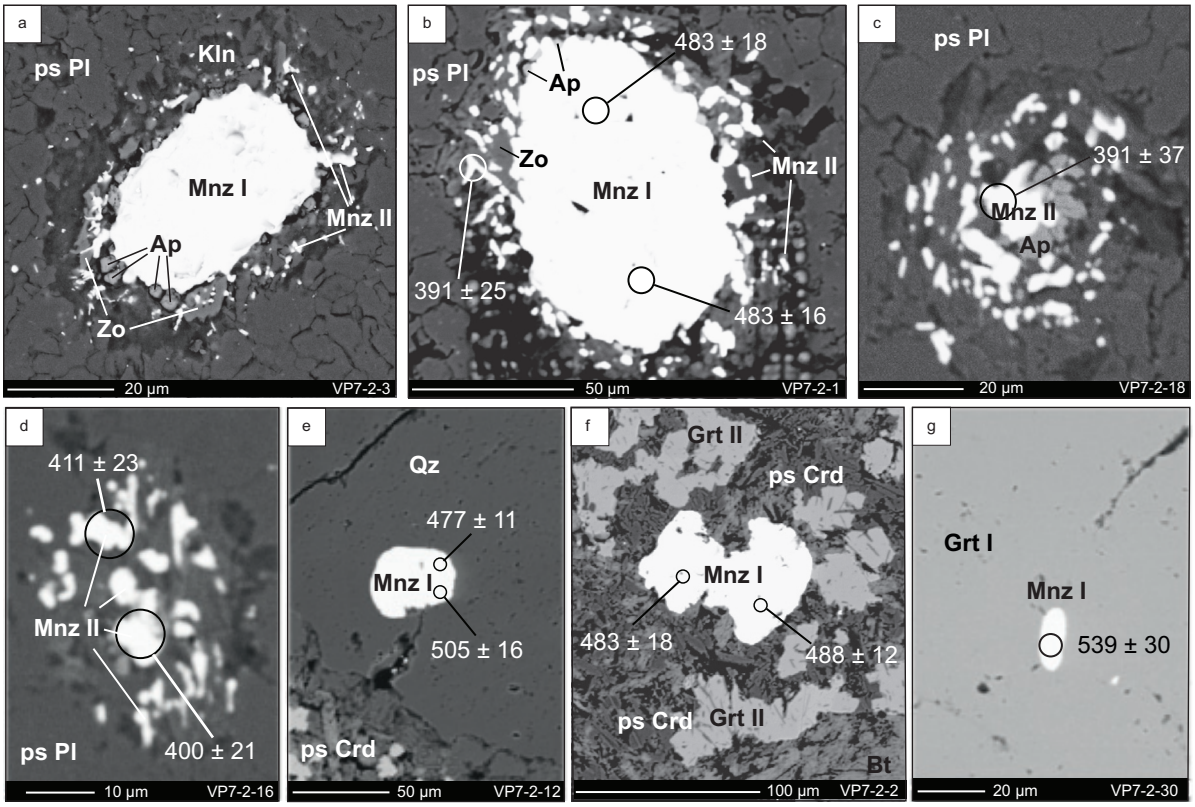

Fig. 3. BSE images of monazite grains from the VP7-2 paragneiss. Circles indicate the location of the LA-ICPMS pits (7 µm diameter) and their corresponding $^{206}Pb/^{238}U$ dates (2σ level). Only consistent dates in both the $^{208}Pb/^{232}Th$–$^{206}Pb/^{238}U$ and $^{206}Pb/^{238}U$–$^{207}Pb/^{235}U$ systems are shown. (a) and (b) Monazite I grain in pseudomorph after plagioclase (ps Pl) with its reaction corona composed of apatite (Ap), zoisite (Zo) and monazite II (Mnz II); (c) and (d) similar coronas in which monazite I has been completely consumed; (e) pristine monazite I included in quartz (Qz); (f) pristine monazite (Mnz I) in pseudomorph after cordierite (ps Crd), consisting of Grt II, cryptocrystalline kyanite and quartz; (g) pristine monazite (Mnz I) included in Grt I. Kln = kaolinite.

samples (Fig. 6a and b). The ThO_2 and UO_2 contents in the core of the reactive monazite are in the range of 3.6–4.7 wt% and 0.3–1.8 wt% respectively. The maximum Y_2O_3 content is significantly higher than in the other samples (up to 3.8 wt%; Fig. 6b). Only one analysis of monazite II gave acceptable results (SM1). It is characterised by a low Th content and relatively high U and Y contents (Fig. 6b).

In conclusion, variations in monazite composition observed between the different samples are mainly related to the protolith (paragneiss *versus* orthogneiss). The different chemical compositions of the monazite crystals in each sample are not clearly related to their textural positions. It is therefore impossible to distinguish the different generations of monazite in samples VP7-2 and VP7r on the basis of their chemical composition. Similarly, the internal zoning observed in pristine monazite or in the core of the reactive monazite is highly variable from grain to grain (SM5) and is not related to their textural position.

The distribution of REE in the monazite of paragneiss sample VP7-2 provides more discriminating information (Fig. 6c and SM3). Pristine monazites (shielded in quartz) have a negative Eu anomaly (Eu/Eu* ≈ 0.13–0.16), and are 10 times more enriched in HREE compared to the core of the reactive monazite I (Eu anomaly ≈ 0.36 to 0.58). One analysis of monazite II shows one of the weakest Eu anomalies (Eu/Eu* ≈ 0.58) and one of the most depleted HREE content (Fig. 6c).

3.2 Textural characteristics of xenotime

Xenotime (YPO_4) is present in two samples (VP7-2 and VP7r). In the orthogneiss sample VP7r, it occurs as 30–50 µm subhedral grains (Fig. 7e, f), with clear evidence that this accessory mineral belongs to the granite magmatic paragenesis. In the paragneiss sample VP7-2, xenotime grains (<30 µm) and numerous µm-sized xenotime inclusions are scattered in large garnet crystals (Fig. 7b-d), which Godard (2009) interpreted as belonging to the HT paragenesis (Garnet I). In contrast, the Ca-rich garnet coronas and overgrowths (Garnet II, Fig. 7a) that formed at the contacts with feldspars during the eclogite-facies metamorphism are devoid of such xenotime inclusions (Fig. 7a-b). Electron microprobe analyses show that the first generation of garnet (Garnet I), coexisting with xenotime, is relatively rich in Y (745 ± 155 µg/g [ppm] Y; 145 spots), which commonly occurs as solid solution of the YAG end-member ($Y_3Al_2[Al_3O_{12}]$) in garnet. By comparison, the eclogite-facies xenotime-free Garnet II is much poorer in it (434 ± 365 µg/g Y; 49 spots).

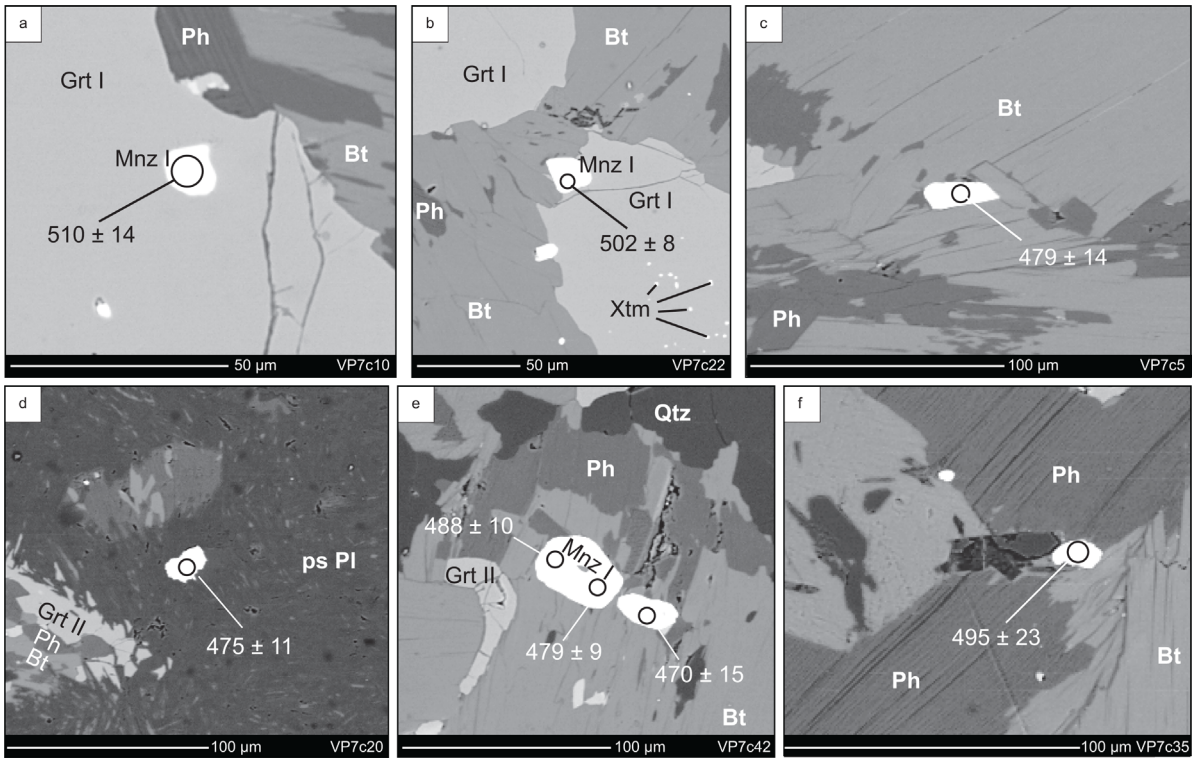

Fig. 4. BSE images of monazite grains from the VP7c paragneiss. Circles indicate the location of the LA-ICPMS pits (7 µm diameter) and their corresponding $^{206}Pb/^{238}U$ dates (2σ level). Only consistent dates in both the $^{208}Pb/^{232}Th$–$^{206}Pb/^{238}U$ and $^{206}Pb/^{238}U$–$^{207}Pb/^{235}U$ systems are shown. (a) Pristine monazite I included in garnet I; (b) open inclusion of monazite I in garnet I in contact with biotite (Bt); note the presence of small inclusions of xenotime (Xtm) in garnet I (see text); (c) pristine monazite I in a matrix of biotite (Bt)/phengite (Ph); (d) monazite I in plagioclase pseudomorph (ps Pl) showing irregular corroded rims; the reaction corona at the monazite-plagioclase interface is not observed in this sample; (e) and (f) pristine monazite I in a matrix of biotite (Bt)/phengite (Ph).

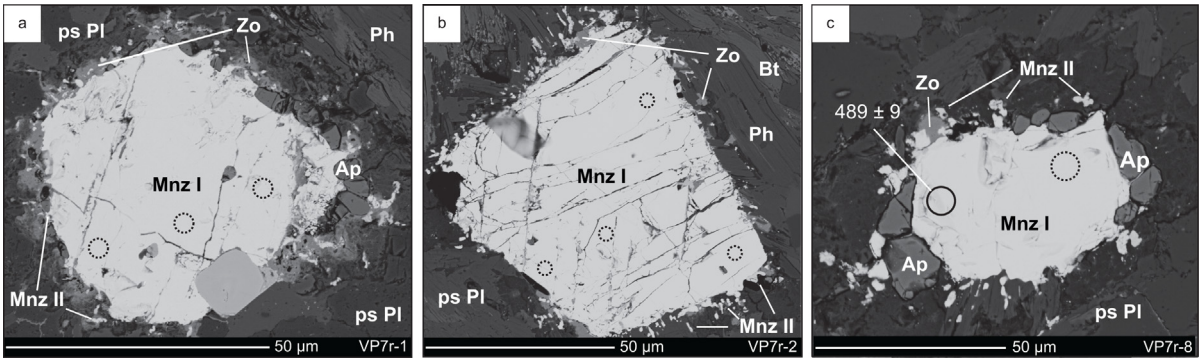

Fig. 5. BSE images of monazite grains from the VP7r orthogneiss. Circles indicate the location of the LA-ICPMS pits (7 µm diameter) and their corresponding $^{206}Pb/^{238}U$ dates (2σ level). Only consistent dates in both the $^{208}Pb/^{232}Th$–$^{206}Pb/^{238}U$ and $^{206}Pb/^{238}U$–$^{207}Pb/^{235}U$ systems are shown; dashed circles indicate the location of the other spot analyses. (a), (b) and (c) Monazite I grains in plagioclase pseudomorphs (ps Pl) with reaction microcoronas composed of apatite (Ap), zoisite (Zo) and monazite II (Mnz II; the small crystals could not be analysed).

This suggests an early crystallization of the xenotime in this sample, coeval with Garnet I. The largest xenotime grains could have been incorporated into Garnet I during its growth, whereas the µm-sized inclusions could have been exsolved during its HT prograde evolution, as the solubility of Y in garnet decreases with temperature (Pyle and Spear, 2000).

4 Monazite and xenotime U-Th/Pb dating

Monazite and xenotime were analysed in thin section by LA-ICPMS in Clermont-Ferrand (France) for U-Th/Pb dating (Figs. 8–10). The analytical methods are presented in the electronic supplementary material SM3. The results are

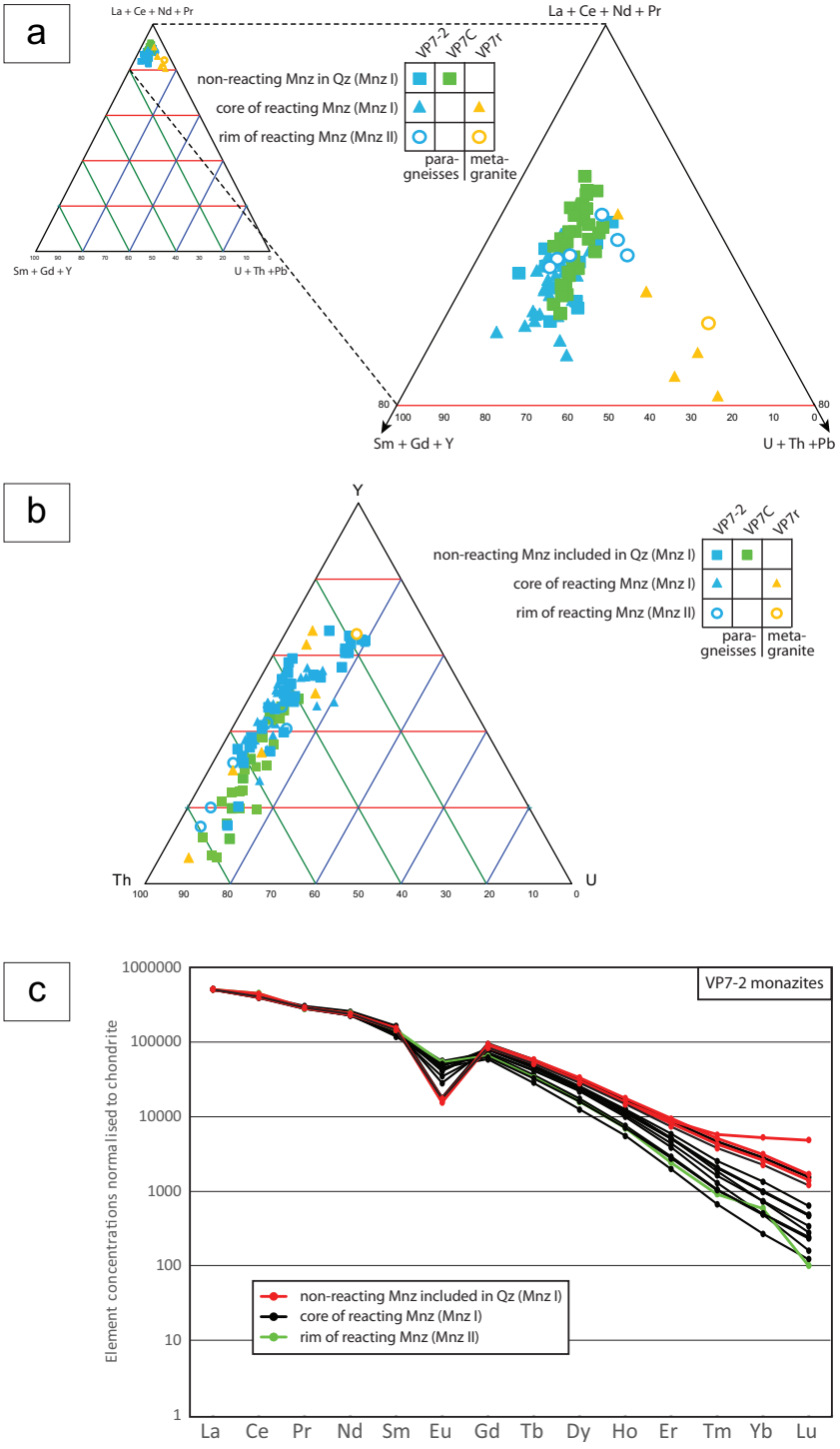

Fig. 6. Chemical composition of monazite from the three studied samples: (a) Ternary diagram La+Ce+Nd+Pr – U+Th+Pb – Sm+Gd+Y (mol%) showing the distribution of the monazite composition amongst the main end-members: monazite *s.s.*, actinide-bearing end-members and mid-heavy REE phosphates; (b) Y-Th-U ternary diagram (mol%) showing the monazite chemical composition in relation to the textural position in each studied sample; (c) chondrite-normalised REE patterns in monazite from the paragneiss sample VP7-2.

presented in Tera-Wasserburg diagrams and U-Th/Pb diagrams (Figs. 8–10). All data are reported in SM2 with 2σ uncertainties.

In monazite, three isotope systems can be used to obtain dates, presented here in order of decreasing reliability: $^{208}Pb/^{232}Th$, $^{206}Pb/^{238}U$ and $^{207}Pb/^{235}U$. ^{232}Th is so abundant (here between 1.5 and 7 wt%; SM1) that ^{208}Pb originated from common Pb can be considered negligible in most cases compared to radiogenic ^{208}Pb. It also enables small spots to be analysed by laser ablation. To ensure that common Pb contamination or isotope disturbance of the Th/Pb system are minimal (Didier *et al.*, 2013), $^{208}Pb/^{232}Th$ dates can be compared with $^{206}Pb/^{238}U$ dates in $^{208}Pb/^{232}Th$ *vs.* $^{206}Pb/^{238}U$

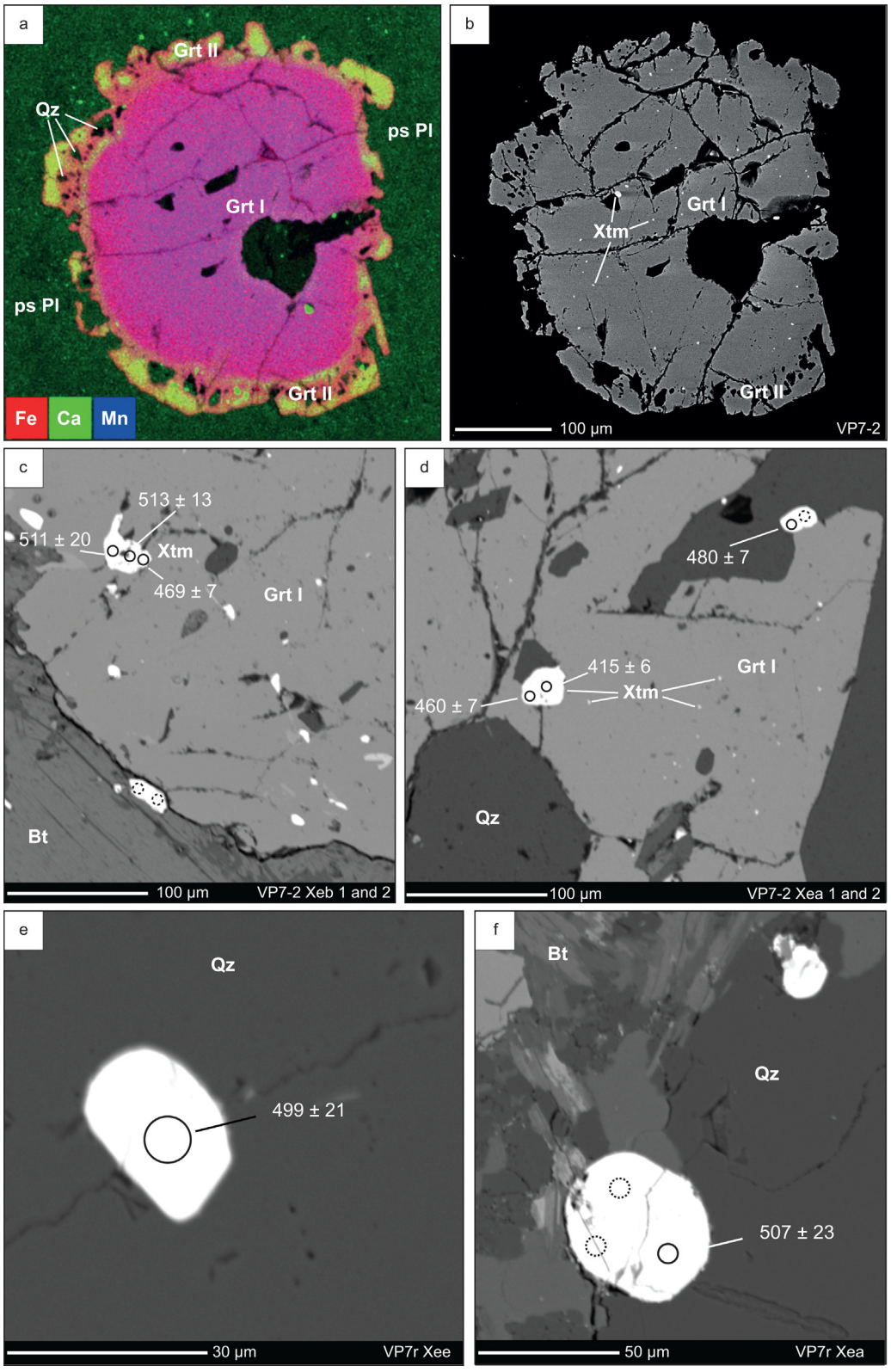

Fig. 7. Images of xenotime from the VP7-2 paragneiss (a-d) and VP7r orthogneiss (e, f). BSE images (b-f) and RGB image (a) with channel intensities correlated to Fe (red), Ca (green) and Mn (blue) contents. Circles indicate the location of the LA-ICPMS pits (7 µm diameter) and their corresponding $^{206}Pb/^{238}U$ dates (2σ level). (a) and (b) Garnet I with an overgrowth of Ca-rich garnet II (Grt II) at the contact with the plagioclase pseudomorph (ps Pl); note that xenotime inclusions are only present in garnet I (see text); (c) and (d) xenotime inclusions in garnet I and in the matrix of the paragneiss sample VP7-2; note the presence of small xenotime inclusions (Xtm) in the garnet core (Grt I); (e) and (f) subhedral xenotime grains (Xtm) in the matrix of the orthogneiss sample VP7r; dashed circles indicate the location of the discordant spot analyses.

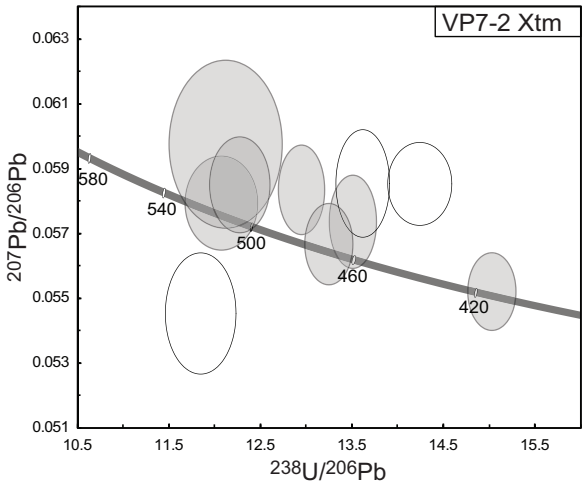

Fig. 8. Xenotime geochronological results for the VP7-2 paragneiss. All data are uncorrected for common Pb. Tera-Wasserburg diagram showing the U/Pb results from xenotime. White ellipses represent discordant data.

diagrams, ^{238}U being the most abundant isotope of U (typically less than 1 wt% in our samples). On the other hand, U/Pb systems are sensitive to common Pb contamination and must be plotted in Tera-Wasserburg diagrams to obtain lower intercept dates consistent with the common Pb composition. In this study, we always compare the results obtained in the three systems and consider as the most geologically significant those results that are consistent in both the ^{208}Pb/^{232}Th-^{206}Pb/^{238}U and ^{206}Pb/^{238}U-^{207}Pb/^{235}U systems.

4.1 Paragneiss sample VP7-2

In sample VP7-2, 6 xenotime grains were analysed for a total of 9 analyses retained after treatment. In this sample, xenotime is present as inclusions in large garnet crystals belonging to the HT paragenesis or close to the dissolved rims of these crystals (Fig. 7c-d). These inclusions are either large (30–40 μm) or μm-sized, the latter possibly resulting from Y exsolution (see 3.2). Only the first category was large enough to be analysed (Fig. 8), and only one grain was analysed in the matrix, outside the garnet. In a Tera-Wasserburg diagram, 3 analyses are discordant and the concordant data range between 516 and 415 Ma. The oldest data are measured in shielded xenotime inclusions in garnet, defining a weighted mean ^{206}Pb/^{238}U date of 509 ± 8 Ma (SM2; MSWD = 0.51; N = 3).

In the same sample, 37 monazite grains were analysed for a total of 106 analyses retained after treatment (63 in monazite II + 43 in monazite I). For the sake of clarity, we show the data obtained from monazites I (*i.e.*, core of reactive monazite and non-reactive pristine monazite included in garnet and quartz; Fig. 9a, b) separately from those obtained from monazite II (*i.e.*, monazite formed in the corona during reaction; Fig. 9c, d). For monazite I, 6 analyses show common Pb contamination, whereas 37 concordant analyses in the Tera-Wasserburg diagram (Fig. 9a) range from 542 to 450 Ma (Fig. 3e-g), the scatter of which prevents the calculation of a concordia date. Twenty-four concordant ^{206}Pb/^{238}U-^{208}Pb/^{232}Th dates spread from 541 to 471 Ma. Twenty analyses are concordant in both the U-Th/Pb and the U/Pb systems and provide a weighted mean ^{206}Pb/^{238}U date of 492 ± 4 Ma (Fig. 9a and SM2; mean square weighted deviation [MSWD] = 2.2; N = 19; 1 data at ~540 Ma excluded) and a weighted mean ^{208}Pb/^{232}Th date of 489 ± 6 Ma (MSWD = 3.6; N = 19; see Fig. 9b for the ^{208}Pb/^{232}Th date distribution). Considering only the pristine monazite (*i.e.*, excluding the core of the reacting monazite grains), the results are similar in the error bar: weighted mean ^{206}Pb/^{238}U date of 490 ± 6 Ma (MSWD = 1.9; N = 11) and weighted mean ^{208}Pb/^{232}Th date of 487 ± 9 Ma (MSWD = 4.2; N = 11).

Most of the monazite II in the reaction corona around the monazite I gives discordant U/Pb dates. The discordance is explained by the small grain size (between 2 and 20 μm) relative to the laser spot size (7 μm), which induces a variable amount of mixing with the adjacent phases (Fig. 3a-d), and the incorporation of various amount of common Pb. Only 13 out of 63 analyses are concordant in both the U/Pb system and the ^{206}Pb/^{238}U –^{208}Pb/^{232}Th system, giving dates between 558 and 388 Ma (Fig. 9c) and a ^{208}Pb/^{232}Th distribution ages defining 2 peaks at about 486 and 398 Ma (Fig. 9d). In a Tera-Wasserburg diagram, 41 analyses define a linear trend intercepting the concordia curve at 395 ± 9 Ma (Fig. 9c; MSWD = 3.1) with a ^{207}Pb/^{206}Pb$_0$ at 0.93 ± 0.27 consistent with the common Pb composition at 395 Ma according to Stacey and Kramers (1975). Five concordant data between 405 and 388 Ma also allow to calculate a U/Pb concordia date of 394 ± 13 Ma (insert of Fig. 9c). The same data give a Th-U/Pb concordia date of 396 ± 6 Ma.

4.2 Paragneiss sample VP7c

Thirty-seven monazite grains were analysed in sample VP7c (Fig. 4) with 37 analyses retained after treatment. Seventeen analyses show common Pb contamination whereas 20 concordant analyses in the Tera-Wasserburg diagram (Fig. 9e) range from 505 to 462 Ma. This spread prevents the calculation of a concordia date. Of these data, 18 are also concordant in the ^{206}Pb/^{238}U –^{208}Pb/^{232}Th system. In a Tera-Wasserburg diagram, 25 data define a linear trend intercepting the concordia curve at 479 ± 4 Ma (MSWD = 1.7; ^{207}Pb/^{206}Pb$_0$ = 0.46 ± 0.27; Fig. 9e). The ^{208}Pb/^{232}Th date distribution confirms the spread of the data and shows two pics at around 495 and 480 Ma (Fig. 9f). The oldest dates in this sample between 510 and 504 Ma were measured in shielded monazite contained in HT garnet crystals (Fig. 4a, SM2).

4.3 Orthogneiss sample VP7r

Ten xenotime grains were analysed in sample VP7r for a total of 12 analyses retained after treatment (Fig. 10b). In this sample, xenotime was observed in the matrix as rounded grains 40 to 50 μm in size (Fig. 7e, f). Three analyses give concordant U/Pb dates between 506 and 440 Ma, the other data showing various amount of common Pb contamination. Five data among the oldest define a linear trend that intercepts the concordia curve at 496 ± 13 Ma (MSWD = 2.3; ^{207}Pb/^{206}Pb$_0$ = 1.25 ± 0.18; Fig. 10b).

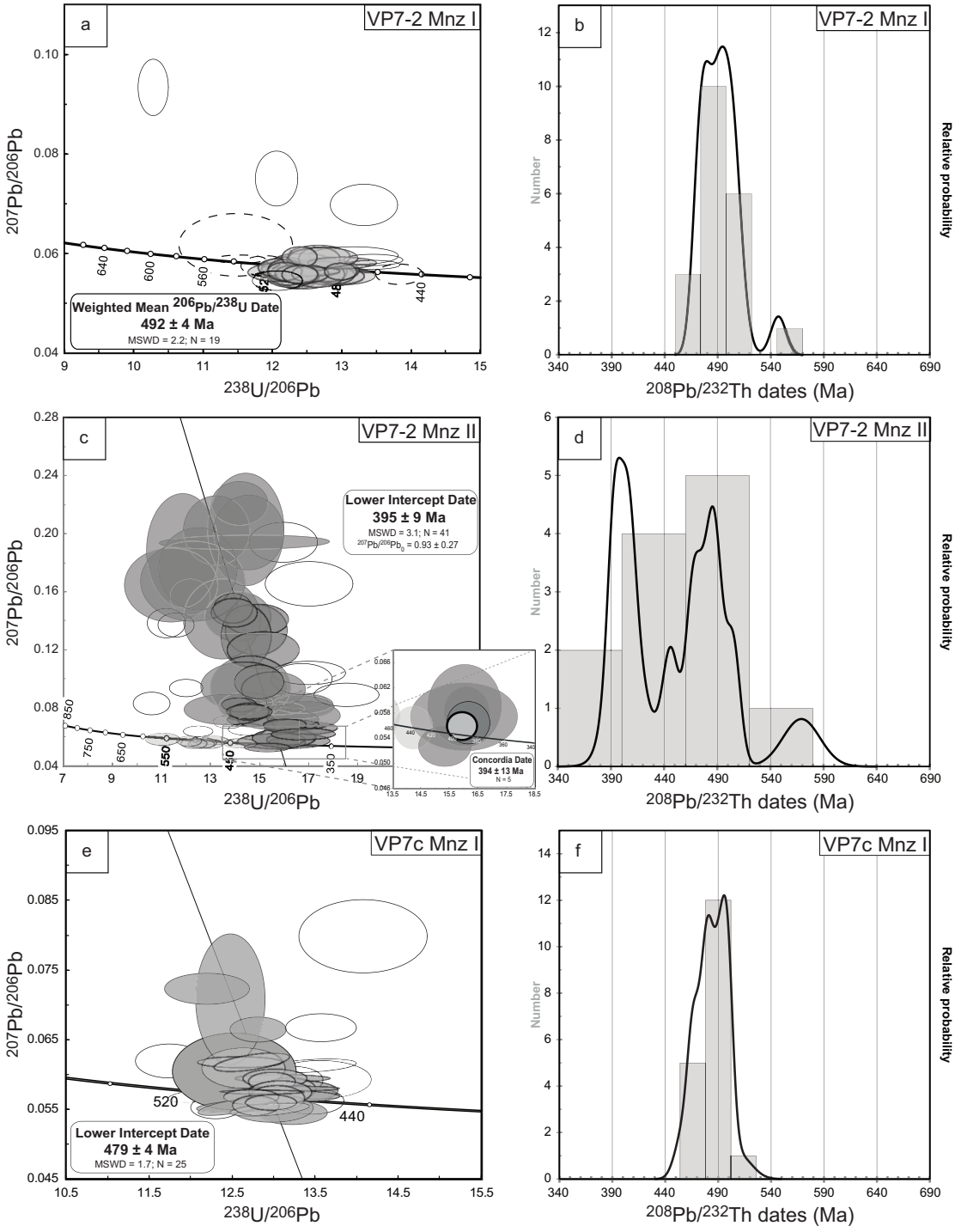

Fig. 9. Monazite geochronological results for the VP7-2 (a-d) and VP7c (e, f) paragneisses. All data are uncorrected for common Pb. (a) Tera-Wasserburg diagram showing the U/Pb results for monazite I. White ellipses correspond to discordant analyses. White dashed ellipses are concordant but were not included in the weighted mean dates calculated from the grey ellipses. (b) Probability histogram of $^{208}Pb/^{232}Th$ dates for monazite I (only concordant data in both the U/Pb systems and the $^{206}Pb/^{238}U$ –$^{208}Pb/^{232}Th$ systems). (c) Tera-Wasserburg diagram showing the U/Pb results for monazite II. Only the dark grey ellipses were taken into account in the free regression calculation. In the inset (concordia date), the light grey ellipse with the bold outline corresponds to the calculated concordia date. (d) Probability histogram of $^{208}Pb/^{232}Th$ dates for monazite II (only concordant data in both the U/Pb systems and the $^{206}Pb/^{238}U$ –$^{208}Pb/^{232}Th$ systems). (e) Tera-Wasserburg diagram showing the U/Pb results in monazite I. White ellipses have not been considered in the free regression calculated with the grey ellipses. (f) Probability histogram of $^{208}Pb/^{232}Th$ dates for monazite I. Only consistent dates in both the $^{208}Pb/^{232}Th$–$^{206}Pb/^{238}U$ and $^{206}Pb/^{238}U$–$^{207}Pb/^{235}U$ systems are shown in (b), (d) and (f).

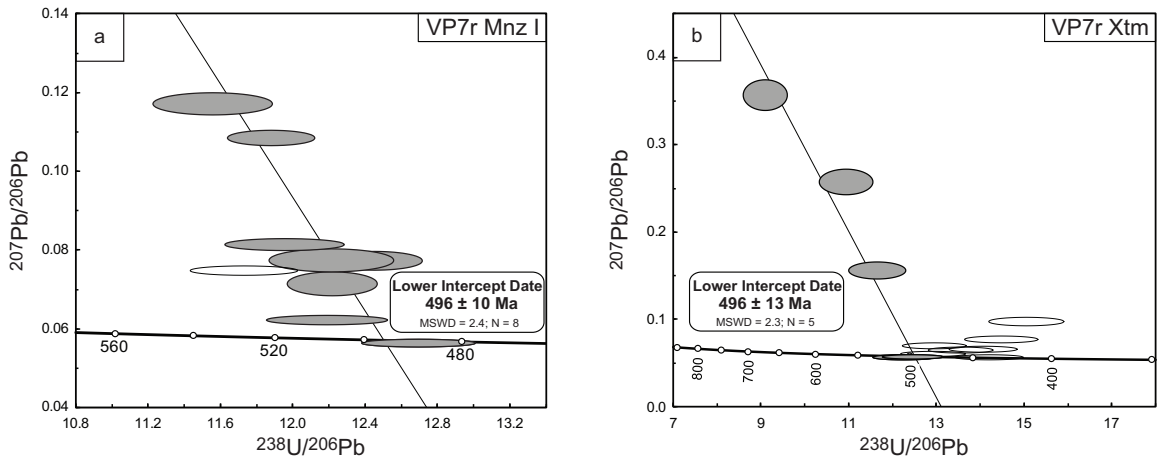

Fig. 10. Monazite and xenotime geochronological results for the VP7r orthogneiss. All data are uncorrected for common Pb. (a) Tera-Wasserburg diagram showing the U/Pb results for monazite I. The white ellipse has not been considered in the free regression calculated with the grey ellipses. (b) Tera-Wasserburg diagram showing the U/Pb results for xenotime. The white ellipses have not been considered in the free regression calculated with the grey ellipses. Only one analysis was consistent in both the $^{208}Pb/^{232}Th$–$^{206}Pb/^{238}U$ and $^{206}Pb/^{238}U$–$^{207}Pb/^{235}U$ systems, so the probability histogram is not available for xenotime in this sample.

Ten monazite grains from the same sample, representing 9 analyses retained after treatment, were measured (Fig. 10a). All but one of the analyses show a common Pb contamination. The concordant data (also concordant in the U-Th/Pb systems) gives a $^{206}Pb/^{238}U$ date of 489 ± 9 Ma (Fig. 5c). In a Tera-Wasserburg diagram, 8 data define a linear trend that intercepts the concordia curve at 496 ± 10 Ma (MSWD = 2.4; $^{207}Pb/^{206}Pb_0 = 0.96 \pm 0.52$; Fig. 10a).

5 Discussion

5.1 Interpretation of the measured dates

In the orthogneiss sample VP7r, the concordant dates obtained for the xenotime grains range up to 506 Ma. Their intercept date at 496 ± 13 Ma (Fig. 10b), although poorly constrained, is similar to that obtained for the monazite I grains at 496 ± 10 Ma (Fig. 10a), with which they are occasionally associated. The age of about 496 Ma is therefore almost certainly that of the granite protolith. This age is close to that obtained for La Roche-aux-Lutins orthogneiss (Rocheservière, Fig. 1) which also belongs to the Les Essarts unit and yielded an Ordovician protolith age of 483 ± 4 Ma (ID-TIMS U-Pb zircon, Lahondère *et al.*, 2009).

In the VP7-2 paragneiss, xenotime is almost exclusively present in the relatively Y-rich garnet crystals that have grown during the HT cycle (Garnet I; see section 3.2). The xenotime dates obtained, despite the small number of analyses, suggest 2 populations at about 509 and 480 Ma (Fig. 8). The xenotime-garnet geothermometer of Pyle and Spear (2000) applied to Garnet I yields temperatures of 534 ± 64°C, in agreement with those of the Garnet I growth estimated by Godard (2009) for the same sample (540→570°C at 0.4 GPa; see A→B in Fig. 13 of Godard, 2009). Since the solubility of Y in garnet decreases with increasing *T* (Pyle and Spear, 2000), the evolution towards the *T* peak up to about 670°C (D in Fig. 13 of Godard, 2009) should result in Y exsolution. Exsolution of Y may have produced the numerous µm-sized xenotime inclusions in Garnet I (Figs. 7b, d and 4b), which are unfortunately too small to be properly analysed, and possibly some overgrowth of the pre-existing xenotime inclusions. It follows that the oldest xenotime age of about 509 Ma provided by the VP7-2 paragneiss should be assigned to the prograde stage of the HT cycle, whereas the second age at about 480 Ma could be related to a readjustment close to the *T* peak (Fig. 11).

The different types of monazite found in the studied samples are related to two main episodes of monazite growth, namely monazite I of Cambro-Ordovician age, similar to the xenotime ages obtained in the same samples, and monazite II of Middle Devonian age (see section 4). In fact, most of the minerals from the initial HT or granitic paragenesis (*i.e.*, biotite, ilmenite, garnet I, cordierite, monazite I) reacted with the plagioclase pseudomorphs during the eclogite-facies metamorphism to produce various coronas (Godard, 2009). Monazite I is simply considered to be one of those minerals that reacted with plagioclase to form, in this case, a corona of apatite + zoisite + monazite II. An important aspect of these HP coronitic reactions is the complete transformation of the HT-LP Ca-rich anorthite end-member of plagioclase into a calcic mineral stable at high pressure. This mineral is a grossular-rich garnet II at the contacts of plagioclase with biotite, ilmenite or garnet I (Figs. 2d, 7a; Godard 2009). At the monazite-plagioclase interface, garnet can hardly crystallise due to the lack of Fe and Mg in both reactants, so apatite and zoisite act as the calcic minerals capable of recycling Ca at high pressure. Although the *P-T* conditions for the formation of this specific corona, unlike other HP coronas, cannot be properly quantified, it is likely to be related to the HP event. Thus, the formation of monazite I and monazite II would coincide with the two main HT and HP events, separated by a first retrogression (Godard, 2009), and therefore related to two different orogenic cycles with a time gap of about 100 Ma.

In the three samples, the Th/Pb and U/Pb dates obtained for monazite I are scattered. Some rare analyses of monazite I

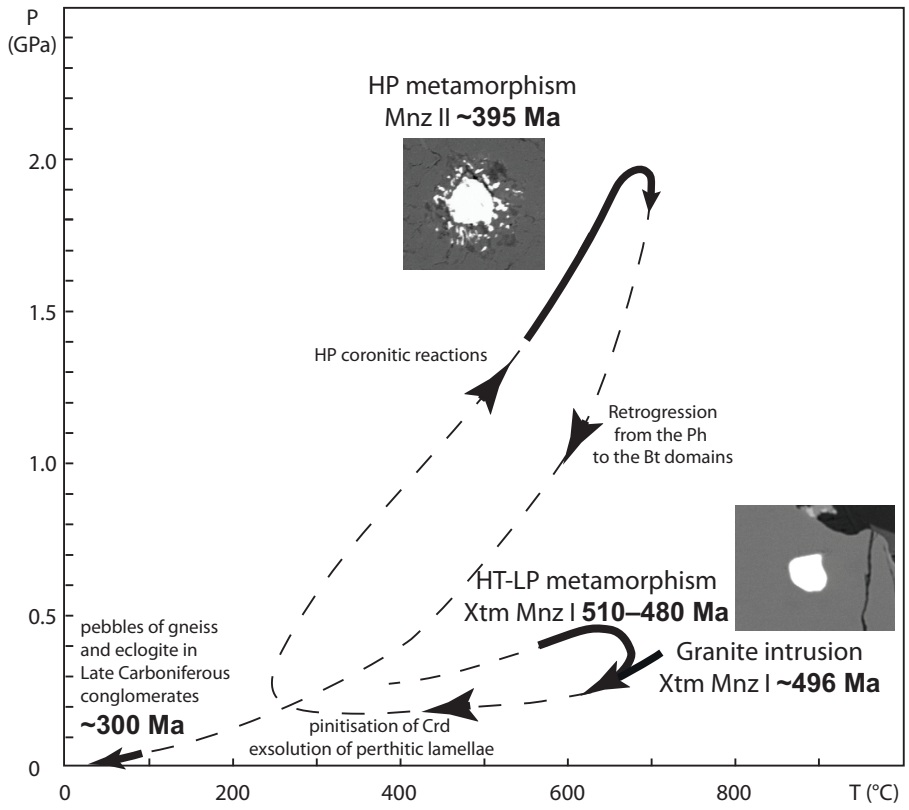

Fig. 11. *P-T*-time path recorded in the VP7 gneisses of Grezay (Les Essarts unit; based on Figure 16 of Godard, 2009). The age range between 510 and 480 Ma is interpreted as monazite I crystallisation and/or re-equilibration during the prograde phase and peak of the HT cycle (paragneiss samples VP7c and VP7-2). Granite emplacement is dated to about 496 Ma in sample VP7r. The HP eclogite-facies event is dated to about 395 Ma by monazite II from the VP7-2 paragneiss. The two BSE images correspond to monazite I included in garnet I of the VP7c paragneiss (Fig. 4a) and crystallized during the HT metamorphic cycle, and to monazite II from the reaction corona formed during the eclogite-facies HP metamorphism at the monazite I-plagioclase interface in the VP7-2 paragneiss (Mnz VP7-2-15; SM2).

(and, incidentally, of monazite II) from paragneiss sample VP7-2 gave dates close to 540–570 Ma (Fig. 9b, d). Assuming that these old ages are geologically significant, they could represent a fraction of detrital monazite inherited from an earlier orogen, Cadomian or Pan-African, since the host rock is a metasediment. Such inheritance is supported by the presence of zones of peculiar composition within certain monazite crystals (*e.g.*, VP7-2-12 in SM5). The other dates of monazite I differ from sample to sample: ~490 and ~480 Ma for paragneiss samples VP7-2 and VP7c, and ~496 Ma for the orthogneiss VP7r, although they are very close within the error bar. In the paragneiss sample VP7-2, textural observations and chemical compositions of the pristine monazite grains do not support the existence of multiple populations among the oldest monazite grains. In the paragneiss sample VP7c, the oldest dates (between 501 and 505 Ma) were obtained for monazite I inclusions armoured in HT garnet I (Fig. 4a), whereas slightly younger ones were obtained for matrix grains (Fig. 4c). This can hardly be explained by mixed dates with younger monazite II-bearing domains, since this sample does not show clear reaction coronas producing monazite II (Fig. 4c, d and f). On the other hand, it may reflect the early trapping of the oldest monazite grains in garnet I, whose growth took place during the prograde stage of the HT metamorphic cycle, at conditions close to 550°C (A→B in Fig. 13 of Godard, 2009). Finally, considering the statistical distribution of pristine monazite Th/Pb dates (concordant in both the $^{206}Pb/^{238}U$-$^{208}Pb/^{232}Th$ and $^{206}Pb/^{238}U$-$^{207}Pb/^{235}U$ systems), two peaks appear at similar values, around 495 and 480 Ma, in both paragneiss samples VP7-2 (Fig. 9b) and VP7c (Fig. 9f), in contrast to the unimodal distribution for monazite I from the VP7r orthogneiss metagranite (496 ± 10 Ma). This suggests that the age of monazite I, which is well defined for the orthogneiss (496 ± 10 Ma), shows a greater spread in the case of the paragneisses (from around 510 to 450 Ma). This spread may indicate monazite crystallization and/or re-equilibration over a longer period during the prograde stage of the HT cycle, close to the *T* peak. This interpretation is also supported by the spread of xenotime ages from the VP7-2 paragneiss (Fig. 8).

Monazite II could only be analysed in paragneiss sample VP7-2 due to its small size in sample VP7r. Most of monazite II yields discordant U-Pb analyses because of mixing with Th and U-poor adjacent phases and incorporation of common Pb during the eclogite-facies metamorphic event. Considering only the concordant data, the Th-U/Pb dates are scattered between 507 and 391 Ma (the concordant date of 562 Ma is considered as inherited from the sedimentary protolith). Concordant $^{208}Pb/^{232}Th$ distribution dates clearly defined 2 peaks at about 486 and 399 Ma (Fig. 9d). This means that in the metamorphic corona surrounding the monazite I, the

measured dates cover the full range of ages from this sample. In other words, some monazite II domains appear to have preserved Cambro-Ordovician ages. The REE profile obtained for a grain of monazite II from sample VP7-2 shows a smaller Eu anomaly and lower HREE contents compared to monazite I in the same rock, which could reflect a crystallisation of monazite II coeval with feldspar breakdown and some garnet growth. A lower intercept date at 395 ± 9 Ma could be obtained with 41 analyses in monazite II and a $^{207}Pb/^{206}Pb$ initial ratio of 0.93 ± 0.27, a value consistent with that of common Pb at 395 Ma, according to Stacey and Kramers (1975). Moreover, concordant data allow the calculation of a concordia age of 394 ± 13 Ma, consistent in the 3 isotopic systems (see section 4.1). We interpret the age of 395 ± 9 Ma as the age of the eclogite-facies event.

5.2 Cambro-Ordovician HT-LP cycle

Godard (2009) has described the petrological characteristics of a HT-LP cycle that resulted, in the Grezay area, in the migmatisation of cordierite-bearing paragneiss and the intrusion of granite. The evolution of the migmatite indicates a clockwise *P–T* path for the HT migmatitic metamorphism, with *T*-peak conditions of about 0.30–0.35 GPa and 650–700 °C (Fig. 11). The data obtained for monazite I and xenotime, although scattered, allow this HT event to be dated to around 510–480 Ma (Late Cambrian-Early Ordovician). As discussed above, this scatter may represent part of the prograde evolution up to the metamorphic peak in the paragneiss, whereas the same minerals give a more precise age of 496 ± 10 Ma for the orthogneiss, which must be attributed to crystallisation of the granite protolith.

During the Cambro-Ordovician, the Armorican Massif lay along the northern margin of Gondwana and was subject to continental extension during the early stages of the Gondwana breakup. Direct evidence of rifting includes widespread emplacement of alkaline/peralkaline magmas (granitoids and volcanics) at *ca.* 490–480 Ma in Brittany, Limousin and in Galicia (Ballèvre *et al.*, 2012; Kroner and Romer, 2013). To explain this Early Ordovician magmatism, Ballèvre *et al.* (2012) proposed a schematic tectonic evolution that favours the opening of an intracontinental rift located away from the volcanic arc and its associated back-arc basin (the Rheic Ocean). In this model, HT metamorphism and partial melting can occur in the lower crust during continental rifting and subsequent opening of the Rheic ocean. If magmatic rocks of Cambro-Ordovician age are relatively common in the western part of the Variscan belt, evidence for metamorphic events of the same age is poorly documented. Abati *et al.* (1999) reported zircon and monazite U/Pb ages between 484 and 500 Ma for the bimodal magmatism and the HT metamorphism recorded in the uppermost unit of the Ordenes Complex (NW Iberia). Monazite U/Pb ages between 498 ± 2 and 484 ± 2 Ma for the metapelitic gneisses have been interpreted to record an upper amphibolite- and granulite-facies metamorphic event shortly after the emplacement of the bimodal magmatic rocks (Abati *et al.*, 1999). Moreover, a metapelitic granulite-facies xenolith hosted by the Monte Castello Gabbro gave, for the same sample, monazite U/Pb ages of 498 ± 2 Ma and rutile U/Pb ages of 391 ± 2 and 382 ± 2 Ma, very similar to our results. More recently, in the Ossa-Morena Complex (SW Iberia), Solís-Alulima *et al.* (2020) dated granite emplacement at 481.2 ± 2.3 Ma and LP partial melting associated with ductile deformation at 477.8 ± 2.4 Ma (SHRIMP zircon U/Pb ages). The authors suggest a common origin for the migmatitic foliation and the La Cardenchosa Pluton emplacement in an extensional environment related to continental rifting.

Eclogites belonging to the same metamorphic unit as the gneisses studied here have yielded zircon with magmatic characteristics and a lower intercept age of 487 ± 12 Ma (Paquette *et al.*, 2017), interpreted as the age of the gabbroic protolith emplaced in an oceanic environment. This age is similar to the youngest age recorded in monazite I from the gneisses. This similarity suggests that the formation of the oceanic gabbros that gave rise to the eclogites occurred at about the same time as the HT-LP metamorphism and granite intrusion in the continental unit, although these two events took place in different geodynamic environments. Godard (1983, 2001) first proposed that the eclogites and altered garnet peridotites (birbirites) represent fragments of a subducted oceanic lithosphere that were later tectonically incorporated into the continental crust during the Variscan collision. The discovery of HP parageneses in the surrounding gneisses (Godard, 2001, 2009) indicates that the tectonic mixing between oceanic and continental crust occurred before or at the same time as their burial in a subduction zone. Unfortunately, we have no information about the time and context that brought these units together, before or during subduction. Similar ages for the oceanic protolith of the eclogites and the HT-LP parageneses of the continental rocks provide a more accurate picture of the geodynamic environment of the oceanic and continental units at that time.

5.3 Eclogite-facies metamorphic event at 395 Ma

The second metamorphic cycle recorded by the studied gneisses occurred under eclogite-facies conditions ($T = 700$°C and $P > 1.6$ GPa) and gave rise to many pseudomorphic and coronitic reactions, as HP parageneses developed at the expense of earlier HT parageneses (Godard, 2009; Fig. 11). So far, the age of the eclogite-facies metamorphism has not been determined (see section 2.1). The paragneiss and orthogneiss samples record the transition from HT to HP parageneses *via* the reaction of monazite I with the HT plagioclase to form monazite II during eclogite-facies metamorphism. Because of their small size, monazite II crystals are not easy to analyse, resulting in a U/Pb age with a large uncertainty. However, we consider the age of 395 ± 9 Ma discussed above as sufficiently robust to represent the age of the HP metamorphism (Fig. 11).

By considering the correlations between the different units exposed in the Ibero-Armorican arc and their structural juxtaposition, Ballèvre *et al.* (2009, 2014) define different groups of tectono-metamorphic units which helps to explain the spread of geochronological data obtained for these units. Like the Champtoceaux unit, the Keramoine and Kergroaz units at Audierne in the South Armorican domain, and the Cabo Ortegal and Sobrado Mellide units in Iberia, the Les Essarts unit belongs to the Upper Allochthon with reference to the Galicia section. According to this model, below the Upper

Allochthon would occur the oceanic complexes of the Middle Allochthon (among which Groix, Dumet and Bois-de-Céné blueschists in the Armorican Massif; *e.g.*, Godard *et al.*, 2024), and then the Lower Allochthon which includes eclogite-bearing units, as the Malpica Tui unit in the Iberia Massif and the Cellier unit in the Armorican Massif. Eclogites from the Lower Allochthon are characterised by a HP-LT metamorphism during the Devonian (370–355 Ma), whereas metabasites from the Upper Allochthon are HP-HT eclogites (or granulites), yielding rather older metamorphic ages of around 400–390 Ma (Ballèvre *et al.*, 2009, 2014). Moreover, geochemical data in the HT eclogitic metabasite rocks from the Upper Allochthon show compositions similar to N-MORB, suggesting an oceanic or arc origin (Montigny and Allègre, 1974; Godard, 1983, 1988, 2001; Bernard-Griffiths and Cornichet, 1985; Gil Ibarguchi *et al.*, 1990; Galàn and Marcos, 1997). By comparison, LT eclogites from the Lower Allochthon are thought to be derived from former dyke swarms intruded into a thinned continental crust (Ballèvre *et al.*, 1994), where orthogneisses with the same reaction microstructures as the Grezay metagranite studied here were metamorphosed under eclogite-facies conditions (*e.g.*, Gyomlai *et al.*, 2023). In the Upper Allochthon, the HP-HT eclogites of the Cabo-Ortegal complex have been dated by an in-situ method to about 390 Ma (scattered SHRIMP U/Pb ages: Ordonez-Casado *et al.*, 2001). In NW Portugal, the Bragança eclogites have yielded zircon and rutile U/Pb ages of 390 ± 4 Ma (ID-TIMS, concordant ages; Roger and Matte, 2005). In the Armorican Massif, HP granulites from the Audierne region (Kergoaz unit) have given zircon ages of 384 ± 6 Ma (ID-TIMS: Paquette *et al.*, 1985). Finally, migmatitic gneisses from the Champtoceaux Unit, containing eclogite lenses, have been dated to about 390 Ma (EMP Th-U/Pb monazite dating; Cocherie *et al.*, 2005), which probably reflects the age of the partial melting, so that the age of the eclogite-facies metamorphism in this unit must be older than 390 Ma (Ballèvre *et al.*, 2009). In the French Massif Central, Sm-Nd dating of the La Bessenoits eclogite has yielded an isochron age of 408 ± 7 Ma (Paquette *et al.*, 1995). Recent geochronological studies have given ages in the same range: garnet Lu/Hf and Sm/Nd ages of 383 ± 1 Ma and 377 ± 3 Ma, respectively, in the Najac eclogite (Lotout *et al.*, 2018); in-situ U/Pb zircon rim of 379 ± 6 Ma and younger ages with garnet Lu/Hf dating at 357 ± 13 Ma and 358 ± 2 Ma in the Levezou eclogites (Lotout *et al.*, 2020); in-situ U/Pb zircon rim of around 380–364 Ma (Berger *et al.*, 2010; Benmammar, 2021) in some Limousin eclogites.

These studies show that the HP metamorphic event in the Upper Allochthon is most likely Lower Devonian in the Iberian-Armorican Arc, and the age of 395 ± 9 Ma obtained for monazite II from the gneisses of Les Essarts Unit is consistent with this conclusion. As pointed out by Ballèvre *et al.* (2014), the HP-HT eclogite metamorphism at 400–390 Ma together with the generation of intraoceanic supra-subduction zone ophiolites at 405–395 Ma in the Upper Allochthon, reflects the first evidence of convergence in the Variscan cycle.

5.4 Consequences for the understanding of the monazite and xenotime chronometers

Monazite is known to be a good tracer of petrological events and a robust geochronometer because of its high Th and, to a lesser extent, U contents, which allow the simultaneous use of three isotopic systems as independent radiometric clocks that control each other (Williams *et al.*, 2007; Bosse and Villa, 2019 and references therein). The low diffusion rate of Pb in the monazite lattice (*e.g.*, Cherniak *et al.*, 2004; Gardés *et al.*, 2006) prevents resetting, even at high temperatures, and its high capability to recrystallise during interactions with fluids and/or during deformation (Wawrzenitz *et al.*, 2012; Didier *et al.*, 2014) makes it a useful geochronometer in polycyclic metamorphic rocks. The present study illustrates these peculiarities very well: on the one hand, the crystallisation of monazite II during the HP metamorphic event, at the expense of HT plagioclase and monazite I, provides direct evidence for the metamorphic reactions taking place in the gneisses during a new orogenic cycle. On the other hand, the limited volume diffusion within the monazite crystal lattice during the *P-T* evolution of the rocks allows the preservation of the ages of the early HT event as well as the record of the HP event. Monazite I isolated from plagioclase shows no textural evidence of reaction and therefore does not record the Early Devonian HP event. The same is observed for xenotime, which is not involved in any reaction. Only the rims of the monazite grains at contact with plagioclase in some samples (VP7-2 and VP7r) are reactive and record the latest metamorphic event. The small-scale processes occurring at the rims are difficult to estimate. From Figure 9c-d, we can see that even in the reaction rims apparent (concordant) dates similar to those obtained from the core of the grains have been measured. Are these relict domains of monazite I or disturbed apparent dates without geological significance? We cannot answer this question in the present case. Unfortunately, current analytical performances do not yet provide sufficient spatial resolution to date small grains with a high degree of accuracy. However, this study shows that the combination of a detailed petrological study and in-situ dating techniques using robust geochronometers can allow complex and superimposed geological events to be approached with sufficient precision.

6 Conclusions

The Les Essarts unit (Armorican Massif, Vendée, France) contains eclogite km-sized lenses within orthogneiss and paragneiss that have preserved traces of an early HT stage (granite intrusion and migmatisation). The monazite and xenotime present in the gneisses make it possible to date the various stages of the polycyclic metamorphic evolution of the unit.

In the three samples studied, monazite I occurs either as inclusions in garnet I (related to the HT event), quartz or biotite in the form of pristine crystals, or at contacts with plagioclase pseudomorphs. In the latter case, monazite I shows complex coronas composed of apatite, zoisite and clusters of small grains of monazite II. Like most minerals of the HT or initial granitic paragenesis, monazite in contact with plagioclase participates in the transition from the HT to the HP event, and therefore records the age of the HP eclogite-facies metamorphism.

In the VP7c paragneiss sample, monazite I gives a lower intercept age of 479 ± 4 Ma, but the concordant U/Pb dates are scattered between 505 and 462 Ma. No clear coronas with monazite II were observed in this sample. Monazite I from paragneiss VP7-2 also shows scattered dates and gives a

weighted mean age of $^{206}Pb/^{238}U$ of 492 ± 4 Ma. Considering the statistical distribution of Th/Pb dates, two peaks appear at similar ages, around 495 and 480 Ma, in the two paragneiss samples, in contrast to the unimodal age distribution for monazite I from the VP7r orthogneiss. This age spread is interpreted as monazite crystallisation and/or re-equilibration over a longer period during the prograde phase of the HT cycle. Xenotime is almost exclusively present as inclusions in garnet I of the VP7-2 paragneiss and records the prograde stage of the HT cycle.

Monazite II consists of small crystals that could only be analysed in paragneiss sample VP7-2, giving concordant ages of about 395 Ma, which we interpret as the age of the eclogite-facies event in the Les Essarts unit. This age is consistent with the results obtained in the HP metamorphic rocks of the Upper Allochthon unit of the Iberian-Armorican Arc (Cabo-Ortegal, Bragança, Audierne and Massif Central).

In the orthogneiss sample VP7r, xenotime and monazite I belong to the magmatic granite paragenesis and indicate the age of the granitic protolith at 496 ± 13 Ma and 496 ± 10 Ma, respectively. Monazite II crystals were too small to be analysed in this sample.

Following Ballèvre *et al.* (2012), HT metamorphism and partial melting are thought to have occurred in the lower crust during continental rifting and the subsequent opening of the Rheic Ocean. The formation of the oceanic gabbros that gave rise to the neighbouring eclogites occurred at about the same time as HT-LP metamorphism and granitic intrusion into the continental unit.

The results presented in this study clearly illustrate the qualities of monazite as a useful geochronometer and a good petrological tracer.

Supplementary material

SM1: EMP analyses in monazite (wt.% and cationic formula for 4 O)

SM2: Th-U/Pb isotopic data of monazite and xenotime

SM3: Trace element analyses of monazite from the sample VP7-2

SM4: Analytical methods

SM5: X-ray element maps of monazite crystals. The maps were acquired at the EPMA by wavelength dispersive spectrometry of Ce (Lα line), Gd (Lβ line), Th (Mα line) and Y (Lα line). Monazite crystals VP7C-40, VP7C-45, VP7-2-12 (all from paragneiss) are pristine monazite (Mnz I) isolated in garnet (Grt I) or quartz (Qz), showing in some cases Th-rich inherited nuclei (VP7C-45, VP7-2-12). Monazite crystals VP7-2-3, VP7-2-7 (from paragneiss), VP7r-1 and VP7r-8 (from orthogneiss) reacted with the hosting plagioclase (ps Pl) to form a Mnz II-bearing corona around a core of preserved Mnz I. Monazite II commonly shows enrichment in Th and Y relative to Mnz I (VP7r-1 and VP7r-8). See also Figures 3e (VP7-2-12), 3a (VP7-2-3), 4a (VP7r-1), 4c (VP7r-8).

The Supplementary Material is available at https://www.bsgf.fr/10.1051/bsgf/2024018/olm.

Acknowledgments

We thank Madame Rémy and her late husband from Grezay for their ever so friendly welcome. Julien Berger and an anonymous reviewer are thanked for their constructive reviews. Marc Poujol and Laurent Jolivet are also thanked for their editorial skills. We would especially like to thank Jean Louis Paquette who, looking at these samples and seeing their petrological complexity, exclaimed: “Why don’t you date a granite instead?”.

Funding

This research received funding from the programme TelluS of the Institut National des Sciences de l’Univers, CNRS, AO09/2009.

References

Abati J, Dunning GR, Arenas R, Dıaz Garcıa F, Gonzalez Cuadra P, Martınez Catalan J, *et al.* 1999. Early Ordovician orogenic event in Galicia (NW Spain): evidence from U-Pb ages in the uppermost unit of the Ordenes Complex. *Earth Planet Sci Lett* 165: 213–228.

Ballèvre M, Marchand J, Godard G, Goujou J-C., Wyns R. 1994. Eo-Hercynian events in the Armorican Massif. In: Keppie JD, ed. Pre-Mesozoic geology in France and related areas. Berlin: Springer, pp. 183–194.

Ballèvre M, Bosse V, Ducassou C, Pitra P. 2009. Palaeozoic history of the Armorican Massif: models for the tectonic evolution of the suture zones. *C R Geosci* 341: 174–201.

Ballèvre M, Fourcade S, Capdevila R, Peucat J-J., Cocherie A, Fanning CM. 2012. Geochronology and geochemistry of Ordovician felsic volcanism in the Southern Armorican Massif (Variscan belt, France): implications for the breakup of Gondwana. *Gondwana Res* 21: 1019–1036. https://doi.org/10.1016/j.gr.2011.07.030.

Ballèvre M, Martínez Catalán JR, López-Carmona A, Pitra P, Abati J, Díez Fernández R, *et al.* 2014. Correlation of the nappe stack in the Ibero-Armorican arc across the Bay of Biscay: a joint French-Spanish project. In Schulmann K, Martínez Catalán JR, Lardeaux JM, Janoušek V, Oggiano G eds. *Geological Society of London Special Publication* 405: 77–113.

Benmammar A. 2021. Comment expliquer la dualité thermique des subductions pré-orogéniques ? : Exemple du métamorphisme de haute-pression dans le Massif central français. Unpublished PhD Thesis, Université Paul Sabatier de Toulouse. 212pp (available online).

Berger J, Féménias O, Ohnenstetter D, Bruguier O, Plissart G, Mercier J-C, *et al.* 2010. New occurrence of UHP eclogites in Limousin (French Massif Central): age, tectonic setting and fluid-rock interactions. *Lithos* 118: 365–382.

Bernard-Griffiths J, Cornichet J. 1985. Origin of eclogites from South Brittany, France: a Sm-Nd isotopic and REE study. *Chem Geol* 52: 185–201.

Bosse V, Féraud G, Ruffet G, Ballèvre M, Peucat J-J., de Jong K. 2000. Late Devonian subduction and early orogenic exhumation of eclogite-facies rocks from the Champtoceaux complex Variscan belt, France. *Geol J* 35: 297–325.

Bosse V, Féraud G, Ballèvre M, Peucat J-J., Corsini M. 2005. Rb-Sr and $^{40}Ar/^{39}Ar$ ages in blueschists from the Ile de Groix (Armorican

Massif, France): implications for closure mechanisms in isotopic systems. *Chem Geol* 220: 21–45.
Bosse V, Villa IM. 2019. Petrochronology and hygrochronology of tectono-metamorphic events. *Gondwana Res* 71: 76–90.
Cenki-Tok B, Oliot E, Rubatto D, Berger A, Engi M, Janots E, *et al.* 2011. Preservation of Permian allanite within an Alpine eclogite facies shear zone at Mt Mucrone, Italy: mechanical and chemical behavior of allanite during mylonitization. *Lithos* 125: 40–50. https://doi.org/10.1016/j.lithos.2011.01.005.
Cherniak DJ, Watson BE, Grove M, Harrison TM. 2004. Pb diffusion in monazite: a combined RBS/SIMS study. *Geochim Cosmochim Acta* 68: 829–840.
Cocherie A, Bé Mézème E, Legendre O, Fanning CM, Faure M, Rossi P. 2005. Electron-microprobe dating as a tool for determining the closure of Th-U-Pb systems in migmatitic monazites, *Amer Mineral* 90: 607–618.
Didier A, Bosse V, Boulvais P, Bouloton J, Paquette JL, Montel JM, *et al.* 2013. Disturbance *versus* preservation of U-Th-Pb ages in monazite during fluid-rock interaction: textural, chemical and isotopic *in situ* study in microgranites (Velay Dome, France). *Contrib Mineral Petrol* 165: 1051–1072.
Didier A, Bosse V, Cherneva Z, Gautier P, Georgieva M, Paquette JL, *et al.* 2014. Syn-deformation fluid-assisted growth of monazite during renewed highgrade metamorphism in metapelites of the Central Rhodope (Bulgaria, Greece). *Chem Geol* 381: 206–222.
Galàn G, Marcos A. 1997. Geochemical evolution of high-pressure mafic granulites from the Bacariza formation (Cabo Ortegal complex, NW Spain): an example of a heterogeneous lower crust. *Geologische Rundschau* 86: 539–355.
Gardés E, Jaoul O, Monte JM, Seydoux-Guillaume AM, Wirth R. 2006. Pb diffusion in monazite: an experimental study of $Pb^{2+} + Th^{4+} \leftrightarrow 2Nd^{3+}$ interdiffusion. *Geochim Cosmochim Acta* 70: 2325–2336.
Gebauer D, Bernard-Griffiths J, Grünenfelder M. 1981. U-Pb zircon and monazite dating of a mafic-ultramafic complex and its country rocks. *Contrib Mineral Petrol* 76: 292–300.
Gil Ibarguchi JI, Mendia M, Girardeau J, Peucat J-J. 1990. Petrology of eclogites and clinopyroxene-garnet metabasites from the Cabo Ortegal Complex (northwestern Spain). *Lithos* 25: 133–162.
Godard G. 1983. Dispersion tectonique des éclogites de Vendée lors d'une collision continent-continent. *Bull Minéral* 106: 719–722.
Godard G. 1988. Petrology of some eclogites in the Hercynides: the eclogites from the southern Armorican massif, France. In: Smith DC, ed. Eclogites and eclogite-facies rocks. Amsterdam: Elsevier, pp. 451–519.
Godard G. 2001. The Les Essarts eclogite-bearing metamorphic complex (Vendée, southern Armorican Massif, France): Pre-Variscan terrains in the Hercynian belt. *Géologie de la France* 2001 (1-2): 19–51 + 2 maps.
Godard G. 2009. Two orogenic cycles recorded in eclogite-facies gneiss from the southern Armorican Massif (France). *Eur J Mineral* 21: 1173–1190.
Godard G, van Roermund HLM. 1995. On clinopyroxene strain-induced microfabrics from eclogites. *J Struct Geol* 17: 1425–1443.
Godard G, Bonnet JY. 2007. Les éclogites et gneiss coronitiques de l'Unité des Essarts (Vendée). Guide d'excursion géologique. *Le Naturaliste vendéen* 7: 3–25, 3 plates.
Godard G, Smith DC, Jaujard D, Doukkari S. 2024. Île Dumet (Armorican Massif, France) and its glaucophane eclogites: the little sister of Île de Groix. *Eur J Mineral* 36: 99–112. https://doi.org/10.5194/ejm-36-99-2024.
Gyomlai T, Yamato P, Godard G. 2023. Petrological study of an eclogite-facies metagranite from the Champtoceaux Complex (La Picherais, Armorican Massif, France). *Eur J Mineral* 35: 589–611. https://doi.org/10.5194/ejm-35-589-2023.
de Hoÿm de Marien L, Pitra P, Poujol M, Cogné N, Cagnard F, Le Bayon B. 2023. Complex geochronological record of an emblematic Variscan eclogite (Haut-Allier, French Massif Central). *J Metamorph Geol* 41: 967–995.
Kroner U, Romer RL. 2013. Two plates – many subduction zones: The Variscan orogeny reconsidered. *Gondwana Res* 24: 298–329.
Lahondère D, Chèvremont P, Godard G, Stussi JM, Bouton P. 2009. Notice de la carte géologique de la France (1/50 000), feuille Palluau (535), 171 p. + annexes (26 p.), BRGM éditions.
Le Bayon B, Pitra P, Ballèvre M, Bohn M. 2006. Reconstructing P-T paths during continental collision using multi-stage garnet (Gran Paradiso nappe, Western Alps). *J Metamorph Geol* 24: 477–496.
Le Breton N, Thompson AB. 1988. Fluid-absent (dehydration) melting of biotite in metapelites in the early stages of crustal anatexis. *Contrib Mineral Petrol* 99: 226–237.
Lotout C, Pitra P, Poujol M, Anczkiewicz R, van Den Driessche J. 2018. Timing and duration of Variscan high-pressure metamorphism in the French Massif Central: a multimethod geochronological study from the Najac Massif. *Lithos* 308-309: 381–394.
Lotout C, Poujol M, Pitra P, Anczkiewicz R, van Den Driessche J. 2020. From burial to exhumation: emplacement and metamorphism of mafic eclogitic terranes constrained through multimethod Petrochronology, case study from the Lévezou Massif (French Massif Central, Variscan Belt). *J Petrol* 61. https://doi.org/10.1093/petrology/egaa046.
Massonne HJ, Li B. 2022. Eclogite with unusual atoll garnet from the southern Armorican Massif, France: pressure-temperature path and geodynamic implications. *Tectonophysics* 823. https://doi.org/10.1016/j.tecto.2021.229183.
Mauler A, Godard G, Kunze K. 2001. Crystallographic fabrics of omphacite, rutile and quartz in Vendée eclogites (Armorican Massif, France). Consequences for deformation mechanisms and regimes. *Tectonophysics* 342: 81–112.
Montigny R, Allègre C. 1974. A? la recherche des océans perdus: les éclogites de Vendée témoins métamorphisées d'une ancienne croÛte océanique. *C R Acad Sci Paris* (D) 279: 543–545.
Nosenzo F, Manzotti P, Poujol M, Ballèvre M, Langlade J. 2021. A window into an older orogenic cycle: P-T conditions and timing of the pre-Alpine history of the Dora-Maira Massif (Western Alps). *J Metamorph Geol* 40: 789–821. https://doi.org/10.1111/jmg.12646.
Ordonez Casado B, Gebauer D, Schäfer HJ, Gil Ibarguchi JI, Peucat J-J. 2001. A single Devonian subduction event for the HP/HT metamorphism of the Cabo Ortegal complex within the Iberian Massif. *Tectonophysics* 332: 359–385.
Paquette J-L., Peucat J-J., Bernard-Griffiths J, Marchand J. 1985. Evidence for old Precambrian relics shown by U-Pb zircon dating of eclogites and associated rocks in the Hercynian belt of South Brittany, France. *Chem Geol* 52: 203–216.
Paquette J-L. 1987. Comportement des systèmes isotopiques U-Pb et Sm-Nd dans le métamorphisme éclogitique. Chaîne hercynienne et chaîne alpine. *Mémoires et Documents du Centre armoricain d'étude structurale des socles* 14: 1–190.
Paquette J-L., Monchoux P, Couturier M. 1995. Geochemical and isotopic study of a norite-eclogite transition in the European Variscan belt: implications for U-Pb zircon systematics in metabasic rocks. *Geochim Cosmochim Acta* 59: 1611–1622.

Paquette JL, Ballèvre M, Peucat JJ, Cornen G. 2017. From opening to subduction of an oceanic domain constrained by LA-ICP-MS U-Pb zircon dating (Variscan belt, Southern Armorican Massif, France). *Lithos* 294-295: 418–437.

Peucat JJ, Vidal P, Godard G, Postaire B. 1982. Precambrian U-Pb zircon ages in eclogites and garnet pyroxenites from South Brittany (France): an old oceanic crust in the West European Hercynian belt? *Earth Planet Sci Lett* 60: 70–78.

Peucat JJ. 1983. Géochronologie des roches métamorphiques (Rb-Sr et U-Pb). Exemples choisis au Groenland, en Laponie, dans le Massif Armoricain et en Grande Kabylie. *Mem Soc Géol Minéral Bretagne* 28: 158.

Pitra P, Poujol M, van den Driessche J, Bretagne E, Lotout C, Gogné N. 2022. Late Variscan (315 Ma) subduction or deceptive zircon REE patterns and U-Pb dates from migmatite-hosted eclogites? (Montagne Noire, France). *J Metamorph Geol* 40: 39–65.

Postaire B. 1983. Systématique Pb commun et U-Pb sur zircons. Applications aux roches de haut grade métamorphique impliquées les dans la chaîne hercynienne (Europe de l'Ouest) et aux granulites de Laponie (Finlande). *Bull Soc Géol Minéral Bretagne* (C) 15: 29–72.

Pyle JM, Spear FS. 2000. An empirical garnet (YAG) – xenotime thermometer. *Contrib Mineral Petrol* 138: 51–58.

Roger F, Matte P. 2005. Early Variscan HP metamorphism in the western Iberian Allochthon – A 390 Ma U-Pb age for the Bragança eclogite (NW Portugal). *Int J Earth Sci* 94: 173–179.

Solís-Alulima B, López-Carmona A, Abati J. 2020. Ordovician metamorphism and magmatism preserved in the Ossa Morena complex: SHRIMP geochronology, geochemistry and Sr-Nd isotopic signatures of the Sierra Albarrana Domain (SW Iberian Massif). *Lithos* 374-375: 105700.

Stacey JS, Kramer JD. 1975. Approximation of terrestrial lead isotope evolution by a two stage model. *Earth Planet Sci Lett* 26: 207–221.

Stevens G, Clemens JD, Droop GTR. 1997. Melt production during granulite-facies anatexis: experimental data from "primitive" metasedimentary protoliths. *Contrib Mineral Petrol* 128: 352–370.

Wawrzenitz N, Krohe A, Rhede D, Romer RL. 2012. Dating rock deformation with monazite: the impact of dissolution precipitation creep. *Lithos* 132-135: 52–74.

Villa IM. 2016. Diffusion in mineral geochronometers: present and absent. *Chem Geol* 420: 1–10.

Waters DJ, Whales CJ. 1984. Dehydration melting and the granulite transition in metapelites from southern Namaqualand, S. Africa. *Contrib Mineral Petrol* 88: 269–275.

Whitney DL, Roger F, Teyssier C, Rey PF, Respaut J-F. 2015. Syn-collapse eclogite metamorphism and exhumation of deep crust in a migmatite dome: the P-T-t record of the youngest Variscan eclogite (Montagne Noire, French Massif Central). *Earth Planet Sci Lett* 430: 224–234.

Williams ML, Jercinovic MJ, Hetherington CJ. 2007. Microprobe monazite geochronology: understanding geologic processes by integrating composition and chronology. *Annu Rev Earth Planet Sci* 35: 137–175.

Cite this article as: Bosse V, Godard G, Devidal JL, Mallens J, Shea T. 2024. Two metamorphic cycles recorded by monazite in eclogite-facies gneisses (Southern Armorican Massif, France): A Cambro-Ordovician continental crust involved in eo-Variscan subduction, *BSGF - Earth Sciences Bulletin* 195: 20.